DUPLICATE

Numerical Weather Prediction

Forecasting Research Technical Report No. 387

RTTOV-7 - SCIENCE AND VALIDATION REPORT

By R.W. Saunders, P. Brunel, F. Chevallier,
G. Deblonde,S.J. English, M. Matricardi, P.J. Rayer.

July 2002

© Crown Copyright 2002

Met Office , NWP Division , Room 344, London Road , Bracknell , Berkshire ,RG12 2SZ,
United Kingdom

Forecasting Research
Technical Report No. 387

RTTOV-7 – SCIENCE AND VALIDATION REPORT

By

Roger Saunders, Pascal Brunel, Frederic Chevallier,
Godelieve Deblonde, Stephen English, Marco Matricardi,
Peter Rayer.

June 2002

The Met Office
NWP Division
Room 344
London Road
Bracknell
RG12 2SZ
United Kingdom

© Crown Copyright 2002

Permission to quote from this paper should be obtained from the above Met Office division

Please notify us if you change your address or no longer wish to receive these publications.

Tel: 44 (0)1344 856245 Fax: 44 (0)1344 854026 email: jsarmstrong@meto.gov.uk

NWP Forecasting Research Technical Report

RTTOV-7 - SCIENCE AND VALIDATION REPORT

by

Roger Saunders[#], Pascal Brunel[+], Frederic Chevallier*, Godelieve Deblonde[$], Stephen English[#], Marco Matricardi[*], Peter Rayer[#] .

[#]*Met Office, London Rd Bracknell, Berks, U.K.*
[+]*MétéoFrance, CMS, Lannion, France.*
[*]*ECMWF, Shinfield Park, Reading, U.K.*
[$]*Meteorological Service Canada, Dorval, Quebec, Canada.*

Abstract

The direct assimilation of satellite radiances into NWP model analyses is now well established and is showing significant improvements in the skill of NWP forecasts. At the heart of the radiance assimilation process is a fast radiative transfer model which allows radiances, corresponding to those measured by a satellite, to be rapidly simulated using the NWP model short range forecast profiles and surface parameters as input. The fast radiative transfer model used at the Met Office in OPS and VAR is RTTOV and this fast model has been upgraded to RTTOV-7 in February 2002. This report describes the scientific changes that have been made to the RTTOV model from the previous version RTTOV-6 and also the results of the various validation tests that were carried out before the code was released to users worldwide by the NWP-SAF. The main upgrades for RTTOV-7 are: much improved simulation of the infrared and microwave water vapour channels, improved microwave surface emissivity model, FASTEM-2, support for AIRS, MODIS and SSM/I(S), and additional RTTOV routines for simulating cloudy radiances.

1. INTRODUCTION AND DOCUMENTATION

The purpose of this report is to document the scientific aspects of the latest version of the NWP SAF fast radiative transfer model, referred to hereafter as RTTOV-7, which are different from the previous model RTTOV-6 and present the results of the validation tests which have been carried out. The enhancements to this version, released in February 2002, have been made as part of the activities of the EUMETSAT NWP SAF. The RTTOV-7 software is available to users on request from the NWP SAF (email: mailto:rttov.nwpsaf@metoffice.com). The RTTOV-7 documentation can be viewed on the NWP SAF web site at: http://www.metoffice.com/research/interproj/nwpsaf/rtm/ and may be updated from time to time. Technical documentation about the software can be found in the RTTOV-7 installation and users guide and RTTOV-7 technical report which are also available and can be downloaded from the RTTOV web site at the link above. The Feb 2002 versions of the documentation are included in the RTTOV-7 distribution file.

The baseline document for the original version of RTTOV is available from ECWMF as Eyre (1991). This was updated for RTTOV-5 (Saunders *et. al.* 1999a, Saunders *et. al.*, 1999b) and for RTTOV-6 with the RTTOV-6 science and validation report hereafter referred to as R6REP2000. Some of the changes for RTTOV-7 are documented in Matricardi *et. al.* (2001) which is referred to below as MM2001. The changes described only relate to the differences from RTTOV-6.

2. SCIENTIFIC CHANGES FROM RTTOV-6 TO RTTOV-7

Only scientific changes between RTTOV-6 and RTTOV-7 are listed here. For technical changes to the software, user interface etc. refer to the RTTOV-7 technical report. The two major technical changes are a rewrite of the code in FORTRAN-90 and a re-organisation of the coefficient file ingest so that there is now one file per sensor which facilitates expansion to new sensors.

2.1 Change to computation of gaseous transmittances

The original basis for the RTTOV fast computation of transmittances is based on Eyre and Woolf (1988). This was successively modified for RTTOV by Eyre (1991), Rayer (1995), Rizzi and Matricardi (1998) and Saunders and Matricardi (1999). In spite of these changes the accurate computation of the water vapour transmittance and the water vapour Jacobian has always been a weakness in RTTOV and this was shown clearly in the intercomparison results of Garand *et. al.* (2001). Related work for IASI fast RT model simulations (Matricardi and Saunders, 1999) showed there was scope to improve on the RTTOV-6 performance for the water vapour channels and this was achieved as described below. More details are given in MM2001.

The simulation of transmittances in RTTOV is based on a regression scheme with a variety of predictors from the profile variables (9 for RTTOV-6) which are related to the layer optical depth, ($d_{i,j}$ - $d_{i,j-1}$), where $d_{i,j}$ is the level to space optical depth from level j and channel i. The regression is actually performed in terms of its departure from a reference nadir profile, $d_{i,j}^{ref}$, for mixed gases, water vapour or ozone. For RTTOV-6 and earlier models the formulation is:

$$d_{i,j} = d_{i,j-1} + Y_j \sum_{k=1}^{K} a_{i,j,k} X_{k,j} + (d_{i,j}^{ref} - d_{i,j-1}^{ref}) \qquad (1)$$

where K is the number of predictors and their definition (i.e. $X_{k,j}$ and Y_j) are given in Tables 1 and 2 of R6REP2000, after removing a common factor, Y_j , to simplify the regression and $a_{i,j,k}$ are the regression coefficients. For RTTOV-7 there is a new set of predictors and the formulation changes slightly to predict the layer optical depth directly rather than as a departure from the reference optical depth:

$$d_{i,j} = d_{i,j-1} + \sum_{k=1}^{K} a_{i,j,k} X_{k,j} \qquad (2)$$

The new predictors are given in Tables 1 and 2 and are a development of those used in RTIASI. For the mixed gases there are now 10 predictors, for water vapour 15 and for ozone 11. This does increase the cost of running the model and a future area of research is to see if the number of predictors can be reduced without significant loss in accuracy. The new formulation in equation 2 arises because the new predictors are defined by taking the ratio with the reference profile (see Table 2) not the differences (see Table 2 of R6REP2000) as for RTTOV-6. This is believed to be one reason for the improved accuracy. Another is that the predictors themselves have been better formulated to simulate water vapour line and continuum absorption. A more detailed description of how the predictors were chosen is given in MM2001. A third difference is that in the computation of the regression coefficients, layers that do not contribute significantly to the top of atmosphere radiance are down-weighted. Finally the coefficients were computed from transmittances for 6 viewing angles in the range 0 to 63.6 deg in contrast to RTTOV-5/6 which were for 5 viewing angles from 0 to 60 deg. This helps to improve the simulation of geostationary imager radiances close to the edge of the earth's disk.

An important advantage of the new set of predictors is that they do a better job in simulating all water vapour channels (infrared and microwave) so that different predictors are not required for each spectral region as was the case for RTTOV-6. In addition they also simulate high resolution infrared radiances to an acceptable accuracy (see 2.6 below).

2.2 Addition of improved microwave surface emissivity model, FASTEM-2

RTTOV-5 and RTTOV-6 included a microwave surface emissivity model FASTEM-1 (English and Hewison, 1998) to compute ocean surface emissivity given a sea surface temperature, surface wind speed and viewing angle for a microwave radiometer channel. This has been successfully used for cross-track scanners (e.g. AMSU) close to nadir but there have been concerns over its simulation of sea surface emissivities for conical scanners (i.e. SSM/I) in particular the sensitivity to wind speed at a combination of low wind speeds and large zenith angles. This was illustrated by Figure 18 of R6REP2000. As a result Deblonde and English (2001) have developed an improved version called FASTEM-2 which does a better job, than FASTEM-1, of taking into account the treatment of non-specular reflection within RTTOV. This has significantly improved the simulation of ocean surface emissivity for SSM/I and AMSU for larger viewing angles as described in Deblonde (2000). The RTTOV-7 code has been developed to allow either FASTEM-1 or FASTEM-2 to be invoked according to the user inputs.

In addition to improving the ocean surface microwave emissivity RTTOV-7 also includes the capability to simulate land/sea-ice microwave surface emissivities. This makes use of 5 coefficients which vary for different land surface types that allow the emissivity as a function of frequency to be computed. The coefficients for different surface types are given in Table 3.

2.3 Inclusion of cosmic background radiation

The microwave 'window' channels can have a significant proportion of downwelling reflected radiation included in the simulated top of atmosphere upwelling radiance. Part of the downwelling component will be cosmic background radiation at a mean radiative temperature of 2.7K. RTTOV-6 and earlier versions assumed this was zero. Table 4 shows the magnitude of the radiance difference between neglecting the cosmic background and including it for SSM/I channels for a cold dry and tropical atmosphere. The differences can be as great as 1.7% in radiance (1.2 degK) for the horizontally polarised 19 GHz channel of SSM/I but is typically a third of this for the vertically polarised channel due to higher surface emissivity. The differences also reduce at the higher frequencies due to higher atmospheric absorption. The inclusion of the cosmic background radiation is only invoked for the microwave channels at present, as its effect is negligible at infrared wavelengths.

2.4 Additional functionality for computing multi-layer cloudy radiances

Prior to RTTOV-7 the computation of cloudy infrared radiances assumed cloud tops at a single pressure level with an effective fractional cloud amount from 0 - 100% (which could include non-unit emissivity). It uses an approximate form of the atmospheric radiative transfer (RT) equation. The top of the atmosphere upwelling radiance, $L(v,\theta)$, at a frequency v and viewing angle θ from zenith at the surface, neglecting scattering effects, can be written as:

$$L(v,\theta) = (1-N)L^{Clr}(v,\theta) + NL^{Cld}(v,\theta) \tag{3}$$

where $L^{Clr}(\nu,\theta)$ and $L^{Cld}(\nu,\theta)$ are the clear sky and fully cloudy top of atmosphere upwelling radiances and N is the fractional cloud cover. The simulation of cloud affected radiances $L^{Cld}(\nu,\theta)$ is computed as:

$$L^{Cld}(\nu,\theta) = \tau_{Cld}(\nu,\theta)\, B(\nu,T_{Cld}) + \int_{\tau_{Cld}}^{1} B(\nu,T)d\tau \tag{4}$$

where $\tau_{Cld}(\nu,\theta)$ is the cloud top to space transmittance and T_{Cld} the cloud top temperature, the emissivity of the cloud top is assumed to be unity which is only valid for optically thick water cloud at infrared radiances.

RTTOV-7 has been enhanced to allow cloud absorption to be taken into account based on the ECMWF broad-band radiation scheme (Morcrette, 1991). Clouds are assumed to be grey bodies, within each channel spectral range, with their contribution to the radiances computed from their horizontal coverage n^i, and their emissivity ε_v^i in each vertical layer i of the user's model. ε_v^i is derived from the cloud liquid and/or ice water path l^i by the relationship:

$$\varepsilon_v^i = 1 - e^{-l^i k_v^i} \tag{5}$$

where k_v^i is the extinction coefficient at frequency v. Its value varies according to the phase of the cloud water, the particle sizes and the temperature. This allows the radiances for semi-transparent cloud to be expressed as a linear combination of $L^{Clr}(\nu,\theta)$ and single layer grey body clouds. The coefficients of the linear combination are functions of the n^i and ε_v^i and depend on the way the cloudy layers overlap. The maximum-random hypothesis (Raïsänen, 1998) is adopted as it explicitly distinguishes between the horizontal coverage and the emissivity of

the cloud layers. Cloud absorption is taken into account in the infrared spectrum following Ebert and Curry (1992) for ice water and Smith and Shi (1992) for liquid water. The water droplet radius is set to 10 μm over land and 13 μm over sea and the ice crystal radii varies between 30 and 60 μm with a temperature dependence from Ou and Liou (1995). Cloud absorption is introduced in the microwave (1-200GHz) as a function of frequency and liquid water/ice content following Hufford (1991) for ice and Liebe *et. al.* (1989) for water clouds. Precipitation effects are not taken into account.

The above calculations are performed in a level above RTTOV in a routine called RTTOVCLD so that the functionality of RTTOV remains the same. More details of this cloud scheme and comparisons with HIRS and MSU are given in Chevallier *et. al.* (2001). Details of how to use the new functionality are given in the users guide and technical report.

2.5 Refinements in Line-by-Line model database

The RTTOV-7 model is based on the same line-by-line (LbL) model transmittances as used for RTTOV-5/6. However since the release of RTTOV-6 several minor problems with these datasets have come to light and have been corrected or clarified as described below.

2.5.1 Infrared transmittances

The level to space infrared transmittances were computed on 43 levels by the GENLN2 model Edwards (1992) using the HITRAN-96 spectral line database and the CKD2.1 water vapour continuum for the 43 diverse TIGR profiles. The infrared line-by-line transmittances from which the fast model RT coefficients are computed did not asymptote to 1 at the top level, but to 0.998, due to an error in the convolution of the infrared channel transmittances. This results in small forward modelling errors (<0.1 degK for HIRS channels) and small unphysical increases in the temperature Jacobians $dBT/dT(p)$ at the top layer (0.1 hPa to space). This error was corrected by recomputing the transmittances for each channel and sensor and a revised set of coefficients was issued for RTTOV-6 in Nov 2000.

With the addition of higher spectral resolution instruments and recently available updated spectroscopic parameters (HITRAN-2000) and water vapour continuum (CKD2.4) it is planned to compute a new set of transmittances from which RTTOV-7 coefficients can be derived. This is planned for later in 2002 and when the transmittances are available the updated coefficients for RTTOV-6 and RTTOV-7 will be available from the RTTOV web site.

2.5.2 Microwave transmittances

For the same TIGR profile dataset, the level to space transmittance for microwave channels were computed using the MPM-89 model for water vapour (Liebe, 1989), the MPM-92 model for oxygen (Liebe *et. al.*, 1992) and the MPM-93 model for the small pressure induced contribution due to nitrogen (Liebe *et. al.*, 1993). The MPM line-by-line calculations on which the original RTTOV-5/6 coefficients were based had performed the channel averaging on the path optical depths rather than on the corresponding transmittances. This provides a source of error in the radiative transfer equation and has therefore been corrected for RTTOV-7 and also for RTTOV-6 in the new set of coefficients issued in Nov 2000. An additional source of error was associated with the original spectral averaging procedure, and has also been removed to ensure the total simulated transmittances are mixed gas multiplied by total/mixed gas transmittance. More details are given in Rayer (2000).

It has also been clarified that the microwave line-by-line code incorporates a mean representation of the Zeeman effect due to the geomagnetic field. Since this representation uses a fixed scalar field strength, independent of latitude and view angle, it will not have removed all the associated variability of transmittance due to the geomagnetic field. This only affects high stratospheric and mesospheric channels (e.g. AMSU-A channel 14 and SSMI(S) channels 19-23).

2.6 Addition of new instruments

Many more infrared and microwave sensors can now be simulated with RTTOV-7 (and most with RTTOV-6 also). The current list of supported instruments and the platforms they are on is listed in Table 5. As the coefficient files are now separated out into one file per sensor this makes adding new sensors relatively easy. Coefficients for RTTOV-6 and RTTOV-7 are available for most of these instruments with some exceptions. Only RTTOV-7 supports FY-1/2, SSMI(S) and AIRS. SSMI(S) includes some mesospheric sounding channels (19-21) which peak close to the upper level of the current 43 level pressure levels (0.1 hPa) employed for RTTOV and so these channels will be inaccurately simulated. Their coefficients are included in the SSMIS coefficient file for completeness. The AIRS file includes all 2378 channels but the initial coefficients released with RTTOV-7 are based on channel responses from the pre-launch tests. A revised set of transmittances will have to be computed post launch with the in-orbit channel responses once they are known. The updated AIRS coefficient file will be made available on the RTTOV web site.

3. Testing and Validation of RTTOV-7

To ensure no bugs have entered in the RTTOV code during the introduction of the above changes an extensive set of tests was applied to the new model before it was released. These tests are described below together with the results of the tests. Not all aspects of the model validation are described in detail here, the microwave surface emissivity model FASTEM-2 validation is described in Deblonde (2000), the gaseous transmittance validation in MM2001 and for cloudy infrared and microwave radiance simulations in Chevallier *et. al.* (2001).

Comparisons can be made with several different sets of profiles with pre-computed LbL transmittances. A set of 43 profiles (42 TIGR/HALOE measured temperature and water vapour profiles plus mean) and 34 NESDIS ozone profiles described in Matricardi and Saunders (1999) was used to generate the transmittance model coefficients for mixed gases, water vapour and ozone and so is termed the dependent set. Secondly an independent set of 117 profiles picked from the ECMWF analyses (Chevallier, 2001) with varying temperature and water vapour from the analyses and ozone from a latitude dependent climatology (Fortuin and Langematz, 1994) was used. Note profiles with surface pressures less than 950 hPa were not included in either sets. A larger subset from the ECMWF analyses was also used for comparisons which included 8987 profiles. Finally several radiosonde based profile datasets were used from TIGR (402 profiles) and Garand *et. al.* (2001) (42 profiles).

The model is validated in several ways:

- The RTTOV-6 and RTTOV-7 gaseous level to space transmittances are compared with the LbL model transmittances for the dependent 43 profile dataset (i.e. those used in the regression). This tests the accuracy of the transmittance model itself.

- The RTTOV-6/7 top of atmosphere radiances are compared with those computed in the same way as in RTTOV but using the LbL model transmittances from the dependent profile sets and in addition the transmittances from the 117 ECMWF profile independent set (Chevallier, 2001). This tests the accuracy of the brightness temperatures simulated by RTTOV-7 assuming no error from the LbL model.

- The RTTOV-6/7 top of atmosphere radiances have been compared with those from other infrared and microwave LbL models to test the accuracy of RTTOV including errors due to the differences between LbL models which are used to train RTTOV-7.

- The RTTOV-6/7 top of atmosphere radiances have been compared with observed ATOVS radiances using NWP analyses to provide the state vector.

- The RTTOV-6/7 Jacobians have been compared for ATOVS channels using the dataset prepared by Garand *et al.* (2001). This allows a comparison with several different models.

- THE RTTOV-7 Jacobians have been compared with SYNSATRAD for HIRS and METEOSAT and with Gastropod for AIRS.

- RTTOV-5/7 plots of $\mathbf{HBH}^{\mathrm{T}}$ from the ECMWF model which show how the background errors map into radiance errors through the Jacobian of HIRS channel 12.

- Validation of the fast surface emissivity models, ISEM-6 and FASTEM

There was also an extensive series of comparisons carried out, not described here, between RTTOV-6 and RTTOV-7 transmittances, radiances, Jacobians and surface emissivities from the direct, TL, AD and K codes to check there are no differences during the code development except those anticipated.

The validation results described below are mainly for ATOVS, SSM/I, SEVIRI and AIRS but the performance of the model for all new instruments is checked in terms of transmittance differences from the LbL model and compared to similar channels in the above sensors.

3.1 Validation of transmittances

3.1.1 ATOVS

As a result of the improved gaseous transmittance prediction scheme described in sec 2.1 changes are observed when comparing the transmittance predictions of RTTOV-6 and RTTOV-7 for HIRS and AMSU channels. The rms of the transmittance differences, defined as (RTTOV-LbL)X100 are shown in Figures 1a-c for a selection of those ATOVS channels most affected by the change from RTTOV-6 to RTTOV-7. These statistics which represent a percentage of unit transmittance, are for 5 different viewing angles in the range 0 to 60 deg. The 43 dependent profile set is used with ozone absorption (which is small for the channels plotted) held constant.

The HIRS water vapour channels are most affected as shown in Figure 1a with significant reductions in rms for RTTOV-7 over RTTOV-6 at all levels especially for HIRS channels 11 and 12. The AMSU-B water vapour channels are shown in Figure 1b with significant improvements in all channels. The AMSU-A stratospheric temperature sounding channels are plotted in Figure 1c and show a slight degradation in the accuracy of the transmittance profiles with RTTOV-7 but the magnitude of the transmittance errors are small and do not lead to significant errors in the top of atmosphere radiances (see below). Note that due to the down weighting of the regression for large optical depths the errors for the new RTTOV-7 predictors asymptote to a value of 0.004% in transmittance compared to zero for the RTTOV-6 scheme.

3.1.2 SSM/I and SSMI(S)

Figure 2a shows the comparison for the SSM/I channels between RTTOV-6 and RTTOV-7 transmittances. In contrast to the ATOVS plots in Figure 1 the remaining plots are for the independent set of 117 ECMWF profiles. For SSM/I and SSMI(S) the differences between the LbL model were only computed for the nominal SSM/I zenith angle of 53.1 deg. For SSM/I the simulations for all the channels are significantly improved especially for the 22.235 GHz channel.

For SSMI(S) only the new AMSU like channels (1-11) are plotted in Figure 2b as the results for the SSM/I like channels (12-18) are very similar to those in Figure 2a (see Table 11 for a definition of SSMI(S) channel numbers). For channels 1-11 the accuracy of the simulations are similar to those plotted in Figures 1b and 1c for AMSU. A plot was also made for the high peaking stratospheric/mesospheric channels (not shown) which gave peaks in standard deviations of transmittance of between 0.1% and 0.3%. However it should be borne in mind that for these channels the LbL values will not be very accurate due to the upper level of the profiles being limited to 0.1 hPa.

3.1.3 MVIRI and SEVIRI

Figure 3a and 3b show the transmittance plots for the METEOSAT-7 MVIRI and MSG-1 SEVIRI channels. Again the accuracy of the transmittance simulations are much improved for RTTOV-7 particularly for the water vapour channels.

3.1.4 AIRS

The new type of sensor included in RTTOV-7 is the high spectral resolution infrared spectrometer AIRS which has 2378 channels. This makes it more difficult to tabulate the accuracy of the transmittance for all channels but Figure 4 attempts to document this by plotting the maximum rms transmittance difference, at all levels, between the LbL model and RTTOV-7 for the 117 ECMWF profile independent set and six zenith angles out to 63.6 deg. Biases are typically less than 10% of the standard deviations. Maximum transmittance errors are normally encountered near the peak of the weighting functions. The larger errors for the water vapour channels in the region 1300-1600 cm^{-1} are evident in this plot. Similar plots for the dependent profile sets are given in MM2001.

3.2 Validation of top of atmosphere radiance

The primary output from RTTOV is the top of atmosphere radiance (expressed as equivalent black body brightness temperature) for each channel and so this is the main parameter by which RTTOV-7 is validated. The brightness temperatures are compared both with those computed from the LbL model used to produce the dependent set transmittances and with brightness temperatures computed from other LbL models. In addition they are also compared with observations using NWP profiles as an input to RTTOV.

3.2.1 Comparison with GENLN2/Liebe MPM computed radiances

This comparison determines the accuracy of the regression scheme itself since the *same* LbL models were used to generate the coefficients. To integrate the radiative transfer along the path, for both dependent and independent profile sets, the RTTOV formulation was used even when the transmittance was computed by the LbL model. This is to ensure any differences are only due to the LbL and fast model transmittances not the integration of the radiative transfer through the atmosphere.

Figure 5 and Tables 6-8 document the comparison between the fast model and LbL brightness temperatures for the 43 dependent profile set and the 117 independent profile set for NOAA-15 ATOVS over six zenith angles in the range 0-63.6 deg. The plot shows the standard deviation of the difference is similar for both profile sets with the exception of AMSU-A channels 10, 13-15 (ATOVS channels 30, 33-35) and some of the AMSU-B channels (ATOVS channels 36-40). For the AMSU-A stratospheric channels and the AMSU-B channels 1 and 2 (ATOVS channels 36-37) the increase in variance is associated only with zenith angles > 60 deg which are never encountered by these instruments in reality. For AMSU-B channel 5 (ATOVS channel 40) the dependent set differences are significantly higher than the independent set. The mean biases (not plotted but tabulated in Tables 6-8) are all less than 0.2K and if only angles less than 60 deg are included this reduces to 0.06K. The biases for the independent set are nearly all greater than the dependent set. Also listed in Tables 6-8 are the ATOVS instrument noise values for each channel which demonstrates the RTTOV-7 errors are now well below the instrument noise for all channels.

The next set of plots in Figure 6a and 6b compare the standard deviations and biases of the fast model minus LbL model NOAA-15 ATOVS radiances for the last three versions of RTTOV (5-7) to show how they have improved with each new version. For these plots the surface emissivity was assumed to be unity for all channels and only 5 angles out to 60 deg were included in the statistics (hence differences with 6 angle/non unit microwave surface emissivity statistics in Figure 5 and Tables 6-8). The major improvement from RTTOV-5 to RTTOV-6 was in the AMSU-B water vapour channels and AMSU-A tropospheric sounding channels. For RTTOV-6 to RTTOV-7 the major improvement has been in the HIRS water vapour and ozone channels although some improvements in the AMSU-B water vapour channels are also evident. In terms of bias plotted in Figure 6b the mean biases of nearly all channels are reduced from RTTOV-5/6 to RTTOV-7.

Equivalent plots for the MSG-1 SEVIRI channels are given in Figure 7a and 7b and Table 9. Both the biases and standard deviations are reduced for all channels. Note the Meteosat MVIRI WV and IR channels correspond to SEVIRI channel numbers 5 and 9 for which similar statistics apply. Note these plots are for 6 zenith angles out to 63.6 deg as these geostationary imager radiances may be associated with angles beyond 70 deg.

Table 10 tabulates the bias and variance for RTTOV-6 and 7 (for SSM/I) for a surface emissivity of 1 (because the cosmic background radiance is included in RTTOV-7). Table 11 tabulates the statistics for a special version of RTTOV-6 (Deblonde, 2001) and RTTOV-7 for SSMI(S). Note only 1 zenith angle is included in the statistics for the RTTOV-7 values (53.1 deg the nominal SSM/I angle) but the RTTOV-6 values include 2 angles either side of 53.1 deg.

The SSMI(S) results are also plotted in Figure 8. In summary the SSM/I channels most influenced by water vapour are improved by a factor of 2 in standard deviation with RTTOV-7 whereas the other channels are simulated with the same accuracy as RTTOV-6. For SSMI(S) the results are not exactly equivalent so caution must be used in interpreting Table 11 and Figure 8. As for SSM/I the window channels (12-18) are improved with the exception of channels 17 and 18 which are slightly degraded. The upper stratospheric/lower mesospheric channels (22-23) are not as well simulated by RTTOV-7 but in this case the transmittances themselves will not be adequate for accurate simulations since there is significant weighting to the optical path above 0.1hPa, the top level. More work is needed to improve the simulation of these mesospheric channels because the Zeeman effect also becomes more significant.

For AIRS the bias and standard deviation of the top of atmosphere brightness temperature differences for the independent profile set are given in Figures 9a and 9b. Biases of up to 0.2K are evident for the ozone and water vapour channels and standard deviations up to 0.3K for a few channels are evident. In general the radiance errors are below the AIRS instrument noise for the majority of channels.

For the accuracy of radiances from other sensors in Table 5 results from similar channels on sensors documented above can be used. For example for AVHRR and other geostationary imagers one can use the MSG-1 SEVIRI values as a guide for the equivalent channels although it should be noted that some of the SEVIRI channels are much broader than AVHRR channels.

3.2.2 Comparison with other radiative transfer model computed radiances

The results described above in *3.2.1* all compare the RTTOV-7 radiances with radiances computed using the same LbL model (i.e. GENLN2/MPM) from which the RTTOV coefficients were generated. Hence errors in the generating models themselves are not included in the above estimates. Several infrared models of various types have been used to compare with various RTTOV simulations. For instance Table 12 gives brightness temperature difference statistics between two models (i.e. MODTRAN and RAD-7 (Merchant, 2001)) for the SEVIRI window channels averaged over 250 TIGR profiles. These statistics can be compared with those in Table 9. With the exception of SEVIRI channel 4 the differences are acceptable with the nadir view RTTOV-7 values between those computed by MODTRAN and RAD-7.

For SEVIRI channel 4 the errors of the RTTOV-7 simulations are greater than 1.5 K when compared with either model. This is believed to be due to the large width of this particular channel (~400 cm^{-1}) which given the single channel approximation in RTTOV means the planck function is only computed at the central frequency. For such wide channels this can introduce errors due to the non-linearity of the Planck function. MM2001 have documented the errors introduced by this approximation for the HIRS channels which can be up to 0.35K for HIRS channel 12 on NOAA-14. In practice the error introduced is nearly all bias so that radiance tuning schemes used at NWP centres can remove this bias before assimilation. This is an area where further developments could be made to RTTOV to reduce this bias particularly for some of the SEVIRI channels.

As an update of the study from Chevallier and Mahfouf (2001) on RTTOV-6, MM2001 have also compared HIRS radiance simulations using RTTOV-6 and RTTOV-7 with the SYNSATRAD model (Tjemkes and Schmetz, 1997) for 8987 profiles selected from the ECMWF model profiles of Chevallier (2001). The Figures and Table from MM2001 are reproduced here for a selection of HIRS and MVIRI channels as Table 13 and Figure 10. This clearly documents the improvements in the HIRS and MVIRI water vapour and ozone channels when compared with SYNSATRAD.

Another comparison has been made with RTTOV simulated AVHRR radiances and those computed by MODTRAN 3.5 on a set of 402 TIGR profiles for all viewing angles and varying surface emissivity over the ocean. This profile set is used for generating AVHRR SST retrieval coefficients for the Ocean and Sea-Ice SAF. The statistics are given in Table 14 and show for the AVHRR channels the standard deviations reduce significantly for all channels and with the exception of channel 3 the biases also reduce.

In the microwave region there are less independent LbL models to compare with. The most comprehensive recent comparison which included RTTOV-6 simulations was the Garand *et. al.* (2001) intercomparison. RTTOV-7 is based on the same LbL model as RTTOV-6 so the results from Garand *et. al.* (2001) can be applied to RTTOV-7 also. The results from Garand *et. al.* (2001) are reproduced here as Table 15 which now includes RTTOV-7. In summary for the four AMSU channels selected the biases with other LbL models are all small (<0.4K) with the exception of AMSU-A channel 14 where there is a large bias due to the inclusion of the Zeeman effect for RTTOV-5/6 but not for the other models. The RTTOV-7 fit to the reference model is slightly 'worse' than RTTOV-6 in all channels although AMSU-18 is the only channel significantly 'worse' but it is not obvious which model is closest to the truth.

Finally the simulated AIRS radiances have been compared for 176 ECMWF independent profiles with the kCARTA LbL model (Strow *et. al.*, 1997) and the Gastropod AIRS fast model (Sherlock, 2001). The latter is based on the kCARTA transmittances. kCARTA is known to include updated spectroscopy which is not in HITRAN-96, primarily different CO_2 line mixing and additional/modified water lines (see Tjemkes *et. al.* 2001) and so some of the differences are due to this. Figure 11 shows the typical radiance differences between Gastropod and RTTOV-7 for the first profile of the set, which are up to 2K for a few points but generally less than 1K. These differences are in line with those found in Tjemkes *et. al.* (2001) between GENLN2 and kCARTA. The differences between Gastropod and kCARTA are also plotted in Figure 11. The main differences between RTTOV-7 and Gastropod are in the bias, less than or equal to 1K across most of the AIRS spectral intervals, while standard deviations are in the range 0.1-0.4K. It is planned to update the GENLN2 spectroscopic dataset in the near future which may improve the comparison with kCARTA.

3.2.3 Comparison with observations

The final validation of the simulated radiances is to compare with real observations. In order to gain a significant number of statistics for a comparison ARPEGE NWP model analysis fields from MétéoFrance are used to provide the atmospheric state vector. The colocations are made with the AAPP(v2.8) HIRS level 1d files which contain HIRS, AMSU and AVHRR radiances mapped to the HIRS fields of view received within the Lannion reception area for the period from May to mid-November 2001. The criteria for the colocation to be included in the statistics are:

- Observation over ocean (which is N.E. Atlantic and Mediterranean)

- Clear sky as defined by >90% clear AVHRR pixels in HIRS fov
- Time difference < 2 hours
- AMSU-A channel 1 < 200 K (to remove coast)
- |RTTOV – Observed| < 20 K (to remove obviously bad data)

This resulted in more than 5700 colocations for all ATOVS sensors. The surface skin temperature is from the AVHRR computed SST and the model fields above 10 hPa are extrapolated which explains the poor results for the stratospheric channels. The surface emissivity is not specified so ISEM-6 or FASTEM-1 (RTTOV-6) and FASTEM-2 (RTTOV-7) values are used. The results plotted in Figures 12a,b,c and d in rms show there is no significant difference between the two models which means other errors introduced during the colocation process dominate.

One comparison with ECMWF NWP model fields plotted in Figure 13 shows the mean scan angle dependence of the observed – model bias for several latitude bands is reduced for the angles away from nadir for RTTOV-7 for HIRS channels 10-12. The global mean time series of the radiance biases for the two models were also examined for the ATOVS channels but although the biases were slightly different for RTTOV-7 compared to RTTOV-5 there was no significant reduction.

3.3 Validation of Jacobians

The accuracy of the Jacobians computed by RTTOV are important to document for the radiance assimilation users as they are instrumental in modifying the NWP model analysis variables. This section describes several different sets of validation results. The most comprehensive comparison of Jacobians with other models was carried out by Garand *et. al.* (2001) which included results from RTTOV-5 and RTTOV-6 along with several LbL models for a selection of HIRS and AMSU channels. The full set of validation results can be viewed at http://www.cmc.ec.gc.ca/rpn/arma/intercomparison/ which provides links to both tables and plots. Garand *et. al.* (2001) showed that RTTOV-6 exhibited some anomalous features in the water vapour Jacobians of HIRS channel 12.

Garand *et. al.* (2001) also present tables of the "goodness of fit" of the fast models to an assigned LbL model in order to summarise how well the analytical values fit the LbL model values computed using the finite difference method. This "goodness of fit" measure, M, can be defined as:

$$M = 100 \sqrt{\frac{\sum_{i=1}^{N} (J_{m,i} - J_{r,i})^2}{\sum_{i=1}^{N} J_{r,i}^2}} \qquad (6)$$

where J_m and J_r are the model and LbL reference Jacobian respectively and the sum is over the number of levels N. The values for M should be treated with caution as spikes in the top level can dominate the value when in fact the general shape of the Jacobian can be good. Nevertheless they provide a useful way to summarise the results. The qualitative guidance is that "goodness of fit" values of less than 10 is good, 10-20 fair and >20 bad.

RTTOV-7 has now been compared with this dataset and the values for M are documented in Table 16 for temperature, water vapour and ozone Jacobians of a selection of HIRS channels for 5 diverse profiles used by Garand *et. al.* (2001). For the HIRS temperature sounding channels (2-5, 15) RTTOV-7 has similar values for M but for the water vapour and ozone channels (9 –12) significant reductions in values for M are evident in both temperature and water vapour or ozone Jacobians. Note in particular the improvements in the water vapour Jacobians for HIRS channel 12. In contrast to RTTOV-6 the values for M are now almost all below 10. For AMSU channels listed in Table 17 there is no significant change between the two models in terms of fit to the MWLBL model Jacobian with the exception of AMSU channel 18. For profiles 19 and 31 the AMSU-18 water vapour Jacobians depart further from the MWLBL values in RTTOV-7 although they are still smooth in shape (unlike for profile 30 where a spike in RTTOV-6 was removed in RTTOV-7). Before deciding whether this is a real degradation the accuracy of the reference MWLBL model needs to be confirmed for this channel.

As the above analysis is only for a few profiles an additional study was performed using SYNSATRAD as a reference which was used to compute Jacobians for 8987 ECMWF model profiles by finite difference for the HIRS ozone and water vapour channels and the Meteosat-7 MVIRI water vapour channel. Mean values for M are tabulated in Table 18 for various latitude bands for HIRS channels 9 and 12 and Meteosat-7 water vapour channel which confirm the improvements in the Jacobians. Figures 14a-14d plot global mean Jacobians for HIRS channel 9 (temperature and ozone) and HIRS channel 12 (temperature and water vapour) where significant improvements in the fit are evident. For HIRS channel 9 there are anomalous features above 400hPa in the RTTOV-6 temperature Jacobian which are removed with RTTOV-7. Also the ozone Jacobian follows the SYNSATRAD values more closely with RTTOV-7. Similarly for HIRS channel 12 the improved fit to the reference Jacobians is evident in both temperature and water vapour which results in the peak of the Jacobians being at a slightly lower level for RTTOV-7.

A study was also made of the RTTOV-7 Jacobians for AIRS as this is a new type of infrared sensor and there was a concern that higher spectral resolution could lead to problems in the simulation. Comparisons were made between RTTOV-7, kCARTA and Gastropod Jacobians. In general the differences were small and can be explained by the different spectroscopy on which the models are based with one exception. As an example Figure 15a plots the ozone Jacobian for AIRS channel 1021 at 1009 cm^{-1} in the ozone absorption band for the first profile of the 117 ECMWF independent set. The Jacobians all peak as expected at 20-40 hPa and there is a reasonable level of agreement between the three models. Figure 15b plots a water vapour Jacobian for an AIRS channel that has an unrealistic structure when RTTOV-7 is compared with Gastropod at low levels. However as this feature is well below the peak of the Jacobian there is no significant effect on the top of atmosphere radiance. It is caused by $\tau_{(mix)}$ becoming very small in the ratio of $\tau_{(mix+wv)}/\tau_{(mix)}$ used to define the water vapour transmittance.

Finally the performance of RTTOV-7 within the ECMWF 4D-Var assimilation system itself has been studied. The matrix transformation $\mathbf{HBH}^{\mathrm{T}}$ allows the model background error covariances in model space **B** (e.g. temperature and specific humidity fields) to be translated into equivalent radiance errors using the Jacobian of HIRS channels **H** and its transpose (see Andersson *et. al.*, 2000 for more details).

As the only upper tropospheric water vapour channel assimilated in the ECMWF model is HIRS channel 12, upper tropospheric water vapour fields in the model are governed primarily by radiances from this channel in data sparse regions. Figure 16a shows the values of HIRS channel 12 background errors computed from $\mathbf{HBH}^{\mathrm{T}}$ for RTTOV-5 over the N. Atlantic using the operational ECMWF 4D-Var system. There are several areas of high implied background error (red is >5K) which are in areas where the atmosphere is very dry. The same plot for RTTOV-7 (which started from the same background fields) in Figure 16b shows that in general the magnitude of these areas of high background errors is reduced which results in a reduced sensitivity to small humidity perturbations in a dry atmosphere. This should result in a better conditioned assimilation of HIRS channel 12 radiances.

3.4 Validation of surface emissivity models

3.4.1 Validation of infrared model, ISEM-6

There have been no changes to the formulation of ISEM-6 and so the results in Sherlock (1999) are still valid. The only issue is for zenith angles greater than 60 deg when using the model outside its intended range. When calculations for the ISEM emissivities were performed for the SEVIRI channels out to 75 deg the computed emissivities varied smoothly from 60 deg to 75 deg and so it was decided to allow calculations to be performed with ISEM-6 beyond 60 deg as for RTTOV-6. Of course the actual values computed may not be strictly valid but it is difficult to check as validation data for these large viewing angles is difficult to obtain.

3.4.2 Validation of new microwave model, FASTEM-2

As described earlier the model FASTEM-2 has been added to RTTOV-7 for improving the simulation of microwave window channels. A detailed assessment of FASTEM-1 and FASTEM-2 is documented in Deblonde (2000) to which the interested reader is referred. In summary for the AMSU channels it was found that FASTEM-2 was more accurate than FASTEM-1. For example when FASTEM 1and 2 were compared, at an angle of 30 deg, with an accurate model for the window channels of AMSU, the maximum bias and standard deviation (in brackets) were <4.7K (2.9K) and <0.75K (0.2K) respectively.

For SSM/I the performance of FASTEM-2 also gives better simulated radiances. As described in R6REP2000 an important quantity for retrieval/radiance assimilation is the sensitivity of the radiances (T_B) to surface wind speed (w_s) as this governs how the measured radiances can influence the model wind speed. Figure 17 compares the sensitivities (dT_B/dw_s) for the SSM/I 19.35 GHz channel for the RTSSMI model (Phalippou, 1996) currently in use operationally at ECMWF and the Met Office for RTM another geometric optics model and for FASTEM-1 and FASTEM-2. The H-polarisation channels are much more sensitive to windspeed than the V-polarisation channels. The wind speed sensitivity for the 19.35 GHz H-pol channel for FASTEM-1 is almost twice the RTSSMI or RTM value at zero windspeed whereas FASTEM-2 is much closer to the other models. All models converge at medium windspeeds (7 m/s) but at high windspeeds RTSSMI has a much greater sensitivity than the other models (3 times at 20 m/s) due to the different specification of the foam cover. Similar results are found for the other channels as documented in Deblonde (2000).

4. Summary and Future Developments

RTTOV-7 has been shown to be an overall improvement to the previous model RTTOV-6 particularly for the infrared water vapour and ozone channels as demonstrated by the various validation results presented in this report. It also supports a wider range of satellite instruments including high resolution infrared sounders. Cloudy infrared and microwave radiances with fractional cloud cover at different levels and different emissivities can also now be modelled using new additional routines now distributed with RTTOV. The modelling of the surface emissivity at microwave frequencies has also been improved.

As part of the NWP-SAF programme more improvements to the model are planned for 2002/3. Possible areas for improvement to be considered for RTTOV-8 are:

- Update infrared line-by-line spectroscopy and include more levels (~80) and better dependent profile set
- Optimisation of number of transmittance predictors for each variable gas
- Improve treatment of wide spectral channels (e.g. SEVIRI channel 4) to reduce bias
- Include NWP model level interface within RTTOV
- Add option of more 'variable' gases (e.g. N_2O, CH_4, CO_2)
- Upgrade to include IASI simulation capability
- Addition of infrared land/ice surface emissivity model
- Improved parametrisation of Zeeman effect
- Addition of reflected solar component
- Improvements to Fortran-90 coding (e.g. more use of STRUCTURES)

Users of the code are invited to submit comments for improvements or report bugs to mailto:rttov.nwpsaf@metoffice.com. An RTTOV email newsgroup exists to share experiences, report bugs and broadcast information on updates to the coefficient files or code. Just send a request to this email to be included on the newsgroup.

5. Acknowledgements

The RTTOV-7 developments and validation described here were carried out as part of the EUMETSAT funded NWP-SAF activities. In addition to the contributions from the main institutes, Met Office, ECMWF and MétéoFrance, there were also contributions from visiting scientists Godelieve Deblonde (MSC) and Tom Kleespies (NESDIS). Thanks are also due to Vanessa Sherlock (NIWA) who provided the input to the Gastropod AIRS results in Figure 15, Erik Andersson (ECMWF) who provided Figure 16 and Graeme Kelly (ECMWF) who provided Figure 13.

6. References

Andersson, E., M Fisher, R. Munro and A. McNally 2000 Diagnosis of background errors for radiances and other observable quantities in a variational data assimilation scheme, and the explanation of a case of poor convergence. *QJRMS,* **126,** *1455-1472.*

Chevallier, F. 2001 TIGR-like sampled databases of atmospheric profiles from the ECMWF 50 level forecast model. NWP-SAF report 1. *NWP SAF Report available from ECMWF librarian.*

Chevallier, F., P. Bauer, G. A. Kelly, C. Jakob, and T. McNally, 2001 Model clouds over oceans as seen from space: comparison with HIRS/2 and MSU radiances. *J. Climate* **14** *4216-4229.*

Chevallier, F. and J-F. Mahfouf, 2001 Evaluation of the jacobians of infrared radiation models for variational data assimilation. *J. Appl. Meteorol.* **40** *1445-1461.*

Deblonde, G. 2000 Evaluation of FASTEM and FASTEM-2. *NWP SAF Report available from RTTOV web site:* http://www.metoffice.com/research/interproj/nwpsaf/rtm/

Deblonde, G. and S.J. English 2001 Evaluation of the FASTEM-2 fast microwave oceanic surface emissivity model. *Tech. Proc. ITSC-XI Budapest, 20-26 Sept 2000 67-78*

Deblonde, G. 2001 Standalone 1DVar scheme for the SSM/I, SSMIS and AMSU. Users guide version 1.0 *NWP SAF Report available from RTTOV web site:* http://www.metoffice.com/research/interproj/nwpsaf/rtm/

Ebert, E.E. and J. A. Curry 1992 A parametrization of ice optical properties for climate models. *J. Geophys. Res.*, **97**, *3831-3836.*

Edwards, D. P., GENLN2: A general line-by-line atmospheric transmittance and radiance model, NCAR Tech. Note NCAR/TN-367+STR, 1992.

English S.J. and T.J. Hewison 1998 A fast generic millimetre wave emissivity model. *Microwave Remote Sensing of the Atmosphere and Environment Proc. SPIE* **3503** *22-30*

Eyre J.R. and H.M. Woolf 1988 Transmittance of atmospheric gases in the microwave region: a fast model. *Applied Optics* **27** *3244-3249*

Eyre J.R. 1991 A fast radiative transfer model for satellite sounding systems. *ECMWF Research Dept. Tech. Memo.* **176** *(available from the librarian at ECMWF).*

Fortuin, J.P.F and U. Langematz 1994 An update on the global ozone climatology and on concurrent ozone and temperature trends. *Proc. SPIE.* **2311** *207-216.*

Garand, L., Turner, D.S., Larocque, M., Bates, J., Boukabara, S., Brunel, P., Chevallier, F., Deblonde, G., Engelen, R., Hollingshead, M., Jackson, D., Jedlovec, G., Joiner, J., Kleespies, T., McKague, D.S., McMillin, L., Moncet, J. L., Pardo, J. R., Rayer, P. J., Salathe, E., Saunders, R., Scott, N. A., Van Delst, P., Woolf, R. 2001 Radiance and jacobian intercomparison of radiative transfer models applied to HIRS and AMSU channels. *J. Geophys. Res.*, **106**, *D20. 24,017-24031.*

Hufford, G. 1991 A model for the complex permittivity of ice. *Int. J. Infrared and Millimeter Waves* **12** *677-681.*

Liebe, H. 1989 MPM- An atmospheric millimeter wave propagation model, *Int. J. of infrared and millimeter waves*, **10**, *631-650.*

Liebe, H., J.T. Manabe and G. Hufford 1989 Millimeter wave attenuation and delay rates due to fog/cloud conditions. *IEEE Trans. Antennas Propag.*, **37**, *1617-1623.*

Liebe, H.J., P.W. Rosenkranz and G.A. Hufford 1992 Atmospheric 60 GHz oxygen spectrum: new laboratory measurements and line parameters. *J. Quant. Spectrosc. Radiat. Transfer* **48** *529-643.*

Liebe, H.J, G.A. Hufford and M.G.Cotton 1993 Propagation modelling of moist air and suspended water/ice particles at frequencies below 1000 GHz. *AGARD 52nd Specialists meeting of the Electromagnetic Wave Propagation Panel, Palace De Mallorca, Spain, 17-21 May 1993.*

Matricardi M and R.W. Saunders 1999 A fast radiative transfer model for simulation of IASI radiances. *Applied Optics* **38** *5679-5691.*

Matricardi, M., F. Chevallier and S. Tjemkes 2001 An improved general fast radiative transfer model for the

assimilation of radiance observations. *ECMWF Research Dept. Tech. Memo.* **345** *(available from the librarian at ECMWF).*

Merchant, C.J. 2001 Radiative transfer model for SEVIRI thermal channels. *Ocean & Sea-Ice SAF Visiting Scientist Report.*

Morcrette, J.J. 1991 Radiation and cloud radiative properties in the ECMWF forecasting system. *J. Geophys. Res.***96** *D5 9121-9132.*

Ou S.-C. and K.-N. Liou 1995 Ice microphysics and climatic temperature feedback. *Atmos. Res.* **35** *127-138.*

Phalippou, L. 1996 Variational retrieval for humidity profile, wind speed and cloud liquid water path with the SSM/I: Potential for numerical weather prediction. *QJRMS,* **122,** 327-356.

R6REP2000 2000 RTTOV-6 Science and Validation report. *NWP SAF report available from RTTOV web site:* http://www.metoffice.com/research/interproj/nwpsaf/rtm/

Räisänen, P. 1998 Effective longwave cloud fraction and maximum-random overlap clouds- a problem and a solution. *Mon. Wea. Rev.* **126** *3336-3340.*

Rayer P.J. 1995 Fast transmittance model for satellite sounding. *Applied Optics,* **34** *7387-7394.*

Rayer, P.J. 2000 Microwave transmittance models for RTTOV. *NWP SAF report available from RTTOV web site*: http://www.metoffice.com/research/interproj/nwpsaf/rtm/

Rizzi, R. and M. Matricardi 1998 The use of TOVS clear radiances for numerical weather prediction using an updated forward model. *QJRMS,* **124** *1293-1312*

Saunders R.W., M. Matricardi and P. Brunel 1999a A fast radiative transfer model for assimilation of satellite radiance observations - RTTOV-5. *ECMWF Research Dept. Tech. Memo.* **282** *(available from the librarian at ECMWF).*

Saunders R.W., M. Matricardi and P. Brunel 1999b An Improved Fast Radiative Transfer Model for Assimilation of Satellite Radiance Observations. *QJRMS,* **125,** 1407-1425.

Sherlock, V.J. 1999 ISEM-6: Infrared Surface Emissivity Model for RTTOV-6. *NWP Tech. Rep. 287 (available from Met. Office Librarian).*

Sherlock, V.J. 2001 Gastropod - a fast radiative transfer model for AIRS and IASI. *NWP Tech. Rep. 362 (available from Met. Office Librarian).*

Smith, E.A. and L. Shi 1992 Surface forcing of the infrared cooling profile over the Tibetan plateau. Part I: Influence of relative longwave radiative heating at high altitude. *J. Atmos. Sci.* **49** *805-822.*

Strow, L.L., H.E. Motteler, R.G. Benson, S.E. Hannon, and S. De Souza-Machado. 1998 Fast computation of monochromatic infrared atmospheric transmittances using compressed look-up tables. *J. Quant. Spectrosc. Rad. Trans.*, **59**, *481-493.*

Tjemkes, S., and J. Schmetz, 1997 Synthetic satellite radiances using the radiance sampling method. *J. Geophys. Res.*, **102**, *1807-1818*

Tjemkes, S. *et. al.* 2001 The ISSWG line-by-line intercomparison experiment. *EUMETSAT Tech. Memo.* **8** *Available from EUMETSAT anonymous ftp server:* ftp.eumetsat.de *in directory /pub/MET/out/LIE*

Predictor	Fixed gases	Water vapour	Ozone
$X_{j,1}$	$sec(\theta)$	$sec^2(\theta) W_r^2(j)$	$sec(\theta) O_r(j)$
$X_{j,2}$	$sec^2(\theta)$	$(sec(\theta) W_w(j))^2$	$\sqrt{sec(\theta) O_r(j)}$
$X_{j,3}$	$sec(\theta) T_r(j)$	$(sec(\theta) W_w(j))^4$	$sec(\theta) O_r(j) \delta T(j)$
$X_{j,4}$	$sec(\theta) T_r^2(j)$	$sec(\theta) W_r(j) \delta T(j)$	$(sec(\theta) O_r(j))^2$
$X_{j,5}$	$T_r(j)$	$\sqrt{sec(\theta) W_r(j)}$	$\sqrt{sec(\theta) O_r(j)}\ \delta T(j)$
$X_{j,6}$	$T_r^2(j)$	$\sqrt[4]{sec(\theta) W_r(j)}$	$sec(\theta) O_r(j)^2 O_w(j)$
$X_{j,7}$	$sec(\theta) T_w(j)$	$sec(\theta) W_r(j)$	$\frac{O_r(j)}{O_w(j)} \sqrt{sec(\theta) O_r(j)}$
$X_{j,8}$	$sec(\theta) \frac{T_w(j)}{T_r(j)}$	$(sec(\theta) W_r(j))^3$	$sec(\theta) O_r(j) O_w(j)$
$X_{j,9}$	$\sqrt{sec(\theta)}$	$(sec(\theta) W_r(j))^4$	$O_r(j) sec(\theta) \sqrt{(O_w(j) sec(\theta)}$
$X_{j,10}$	$\sqrt{sec(\theta)}\ \sqrt[4]{T_w(j)}$	$sec(\theta) W_r(j) \delta T(j) \lvert \delta T(j) \rvert$	$sec(\theta) O_w(j)$
$X_{j,11}$	0	$(\sqrt{sec(\theta) W_r(j)}) \delta T(j)$	$(sec(\theta) O_w(j))^2$
$X_{j,12}$	0	$\frac{(sec(\theta) W_r(j))^2}{W_w}$	0
$X_{j,13}$	0	$\frac{\sqrt{(sec(\theta) W_r(j)} W_r(j)}{W_w(j)}$	0
$X_{j,14}$	0	$sec(\theta) \frac{W_r^2(j)}{T_r(j)}$	0
$X_{j,15}$	0	$sec(\theta) \frac{W_r^2(j)}{T_r^4(j)}$	0

Table 1: RTTOV-7 predictors for mixed gases, water vapour and ozone used in equ.2. The profile variables are defined in Table 2. j is the jth layer which is the layer above level j where the level number starts at 0 for the top of atmosphere.

$$T(j) = [T^{profile}(j) + T^{profile}(j-1)] / 2 \qquad T^*(j) = [T^{reference}(j) + T^{reference}(j-1)] / 2$$

$$W(j) = [W^{profile}(j) + W^{profile}(j-1)] / 2 \qquad W^*(j) = [W^{reference}(j) + W^{reference}(j-1)] / 2$$

$$O(j) = [O^{profile}(j) + O^{profile}(j-1)] / 2 \qquad O^*(j) = [O^{reference}(j) + O^{reference}(j-1)] / 2$$

$P(j) = [Pres(j)]$ *where this is the pressure at each layer lower boundary. Pres(1)=0.1 coincides with the lower boundary of layer 1 (bounds are 0.005 and 0.1 hPa).*

$$T_r(j) = T(j) / T^*(j) \qquad \delta T(j) = T(j) - T^*(j) \qquad W_r(j) = W(j) / W^*(j)$$

$$O_r(j) = O(j) / O^*(j)$$

$$T_w(j) = \sum_{l=2}^{j} P(l)[P(l) - P(l-1)]T_r(l-1)$$

$$W_w(j) = \left\{\sum_{l=1}^{j} P(l)[P(l) - P(l-1)]W(l)\right\} / \left\{\sum_{l=1}^{j} P(l)[P(l) - P(l-1)]W^*(l)\right\}$$

$$O_w(j) = \left\{\sum_{l=1}^{j} P(l)[P(l) - P(l-1)]O(l)\right\} / \left\{\sum_{l=1}^{j} P(l)[P(l) - P(l-1)]O^*(l)\right\}$$

The $Pres(j)$'s are the values of the pressure at each layer boundary.

$T^{profile}(j)$, $W^{profile}(j)$ and $O^{profile}(j)$ are the temperature, water vapour mixing ratio and ozone mixing ratio profiles. $T^{reference}(j)$, $W^{reference}(j)$ and $O^{reference}(j)$ are corresponding reference profiles. For these variables j refers to the jth level; otherwise j is the jth layer, i.e.the layer above the jth level. Note that $P(0) = 2P(1) - P(2)$ and $T_w(1) = 0$.

Table 2: Definition of profile variables used in predictors defined in Table 1.

	Coefficients for FASTEM-2				
	1	2	3	4	5
	Summer land surface				
Forest	1.7	1.0	163.0	0.0	0.5
Open Grass	2.2	1.3	138.0	0.0	0.42
Bare soil	2.3	1.9	21.8	0.0	0.5
	Winter land surface				
Forest and snow	2.9	3.4	27.0	0.0	0.0
Deep dry snow	3.0	24.0	60.0	0.1	0.15
Frozen soil	117.8	2.0	0.19	0.2	0.35
	Sea ice				
Grease ice	23.7	7.7	17.3	0.0	0.15
Baltic nilas	1.6	3.3	2.2	0.0	0.0
New ice (no snow)	2.9	3.4	27.0	0.0	0.0
New ice (snow)	2.2	3.7	122.0	0.0	0.15
Brash ice	3.0	5.5	183.0	0.0	0.0
Compact pack ice	2.0	1,700,000	49,000,000	0.0	0.0
Fast ice	1.5	77.8	703	0.1	0.35
Lake ice + snow	1.8	67.1	534	0.1	0.15
Multi-year ice	1.5	85,000	4,700,000	0.0	0.0

Table 3. Coefficients for FASTEM-2 for different surface types (adapted from English and Hewison, 1998).

SSM/I chan	19 GHz V	19GHz H	22GHz V	37 GHz V	37 GHz H	85 GHz V	85 GHz H
Tropical Prof	0.3%	0.7%	0.2%	0.2%	0.5%	0.02%	0.06%
Arctic Prof	0.5%	1.7%	0.4%	0.3%	1.1%	0.1%	0.4%

Table 4 Effect of cosmic background radiation on SSM/I channels. Values tabulated are the percentage change in radiance including the cosmic background minus those without for 2 extreme profiles over the ocean.

Platform	RTTOV id	Sat id range
NOAA	1	2 to 17
DMSP	2	8 to 16
Meteosat	3	2 to 7
GOES	4	8 to 12
GMS	5	5
FY-2	6	2
TRMM	7	1
ERS	8	1 to 2
EOS	9	1 to 2
ENVISAT	11	1
MSG	12	1
FY-1	13	3 to 5

Sensor	RTTOV id	Channels
HIRS	0	1 to 19
MSU	1	1 to 4
SSU	2	1 to 3
AMSU-A	3	1 to 15
AMSU-B	4	1 to 5
AVHRR	5	3b to 5
SSMI	6	1 to 7
VTPR1	7	1 to 8
VTPR2	8	1 to 8
TMI	9	1 to 9
SSMIS	10	1 to 24*
AIRS	11	1 to 2378
MODIS	13	1 to 17
ATSR	14	1 to 3
MVIRI	20	1 to 2
SEVIRI	21	4 to 11
GOES-Imager	22	1 to 4
GOES-Sounder	23	1 to 18
GMS imager	24	1 to 2
FY2-VISSR	25	1 to 2
FY1-MVISR	26	1 to 3

**channels 19-21 are not simulated accurately*

Table 5. Platforms and sensors supported by RTTOV-7 as at 1 June 2002. Sensors in italics are only supported by RTTOV-7.

HIRS		RTTOV-7 43 dependent set			RTTOV-7 117 independent set		
Channel #	NeDT degK	Mean bias degK	St. dev. degK	Max diff degK	Mean bias degK	St. dev. degK	Max diff degK
1	2.77	0.00	0.04	0.26	0.00	0.03	0.12
2	0.74	0.00	0.02	0.06	-0.01	0.01	0.06
3	0.55	0.00	0.02	0.13	0.00	0.01	0.06
4	0.31	0.00	0.03	0.12	0.01	0.02	0.17
5	0.18	-0.01	0.04	0.17	0.03	0.03	0.24
6	0.18	0.00	0.03	0.10	0.01	0.03	0.13
7	0.14	0.00	0.05	0.12	0.00	0.05	0.20
8	0.06	0.00	0.01	0.03	0.00	0.02	0.11
9	0.13	0.00	0.06[+]	-	0.08	0.09	0.25
10	0.17	0.00	0.04	0.14	-0.03	0.06	0.30
11	0.44	0.00	0.09	0.32	-0.04	0.09	0.35
12	0.96	0.00	0.11	0.56	-0.07	0.14	1.01
13	0.10	0.00	0.02	0.05	0.01	0.02	0.12
14	0.10	0.00	0.02	0.05	0.01	0.02	0.06
15	0.24	0.00	0.02	0.09	0.01	0.02	0.11
16	0.31	0.00	0.03	0.10	0.02	0.02	0.10
17	0.15	0.00	0.01	0.03	0.01	0.01	0.04
18	0.04	0.00	0.01	0.02	0.00	0.01	0.02
19	0.02	0.00	0.01	0.03	0.00	0.02	0.21

[+]Value computed from 34 NOAA ozone dependent profile set

Table 6. NOAA-15 HIRS brightness temperature statistics for RTTOV-7 minus LbL values for 43 TIGR profile dependent set and EC 117 independent profile sets for 6 angles out to 63.6 deg.

AMSU-A		RTTOV-7 43 dependent set			RTTOV-7 117 independent set		
Channel #	NeDT degK	Mean bias degK	St. dev. degK	Max diff degK	Mean bias degK	St. dev. degK	Max diff degK
1	0.20	0.00	0.01	0.04	-0.01	0.01	0.05
2	0.24	0.00	0.01	0.04	-0.02	0.03	0.15
3	0.19	0.00	0.02	0.08	-0.02	0.03	0.19
4	0.13	0.00	0.01	0.06	0.01	0.01	0.07
5	0.13	0.00	0.01	0.03	0.02	0.01	0.08
6	0.11	0.00	0.01	0.03	0.01	0.01	0.06
7	0.12	0.00	0.01	0.02	0.00	0.01	0.03
8	0.13	0.00	0.00	0.01	0.00	0.00	0.01
9	0.15	0.00	0.01	0.03	-0.01	0.01	0.08
10	0.19	-0.01	0.02	0.08	0.20	0.16	0.40
11	0.20	-0.01	0.04	0.20	0.00	0.04	0.28
12	0.31	-0.02	0.06	0.27	-0.02	0.07	0.46
13	0.42	-0.02	0.04	0.19	-0.05	0.09	0.59
14	0.70	-0.01	0.02	0.11	-0.04	0.06	0.41
15	0.10	0.00	0.05	0.17	0.07	0.11	0.34

Table 7. NOAA-15 AMSU-A brightness temperature statistics for RTTOV-7 minus LbL values for 43 TIGR profile dependent set and EC 117 independent profile sets for 6 angles out to 63.6 deg.

AMSU-B		RTTOV-7 43 dependent set			RTTOV-7 117 independent set		
Channel #	NeDT degK	Mean bias degK	St. dev. degK	Max diff degK	Mean bias degK	St. dev. degK	Max diff degK
1	0.32	0.00	0.05	0.16	0.07	0.11	0.35
2	0.71	0.00	0.07	0.24	-0.01	0.09	0.74
3	1.05	0.00	0.03	0.14	-0.01	0.07	0.83
4	0.69	0.01	0.04	0.16	-0.01	0.04	0.44
5	0.57	-0.01	0.10	0.66	0.00	0.05	0.40

Table 8. NOAA-15 AMSU-B brightness temperature statistics for RTTOV-7 minus LbL values for 43 TIGR profile dependent set and EC 117 independent profile sets for 6 angles out to 63.6 deg.

SEVIRI	RTTOV-6			RTTOV-7		
Channel # (wavelength)	Mean bias degK	St. dev. degK	Max diff degK	Mean bias degK	St. dev. degK	Max diff degK
4 3.9μm	-0.05	0.04	0.26	0.00	0.01	0.08
5 6.2μm	0.22	0.79	2.61	-0.07	0.18	1.07
6 7.3μm	0.24	0.57	1.83	-0.03	0.11	0.37
7 8.7μm	-0.12	0.19	0.88	0.01	0.04	0.26
8 9.7μm	0.35	0.34	1.14	0.31	0.11	0.54
9 10.8μm	-0.09	0.10	0.53	0.00	0.01	0.08
10 12.0μm	-0.12	0.13	0.68	-0.01	0.03	0.19
11 13.4μm	-0.18	0.12	0.66	-0.10	0.07	0.32

Table 9 MSG-1 SEVIRI brightness temperature difference statistics for RTTOV-6 and 7 minus LbL values for ECMWF 117 independent profile set. The surface emissivity was set to unity and the values include 6 zenith angles from zero to 63.6 deg.

SSM/I	RTTOV-6			RTTOV-7		
Channel # Frequency	Mean bias degK	St. dev. degK	Max diff degK	Mean bias degK	St. dev. degK	Max diff degK
1 19V	-0.004	0.013	0.037	0.007	0.007	0.034
2 19H	-0.004	0.013	0.037	0.007	0.007	0.034
3 22V	-0.010	0.039	0.121	0.010	0.009	0.036
4 37V	0.003	0.011	0.032	0.014	0.008	0.037
5 37H	0.003	0.011	0.032	0.014	0.008	0.037
6 85V	-0.039	0.032	0.158	-0.013	0.016	0.051
7 85H	-0.039	0.032	0.158	-0.013	0.016	0.051

Table 10. SSM/I brightness temperature difference statistics for RTTOV-6 and 7 minus LbL model values for ECMWF 117 independent profile set. The surface emissivity was set to unity and the values are all for one zenith angle of 53.1 deg.

	RTTOV-6 (2 angles) TIGR 43 profiles		RTTOV-7 (1 angle) ECMWF 117 profiles		
Channel # (frequency)	St. dev. degK	Max diff degK	Mean bias degK	St. dev. degK	Max diff[1] degK
1 50.3GHz	0.028	-0.093	0.002	0.025	0.122
2 52.8GHz	0.007	0.023	0.000	0.007	0.023
3 53.5GHz	0.010	-0.026	-0.006	0.008	0.036
4 54.4GHz	0.006	0.017	-0.006	0.007	0.035
5 55.5GHz	0.002	-0.006	-0.003	0.004	0.011
6 57.3GHz	0.006	-0.028	-0.033	***0.032***	0.081
7 59.4GHz	0.026	-0.084	-0.010	0.029	0.240
8 150GHz	0.097	0.347	0.004	0.065	0.477
9 183.3GHz	0.054	0.161	0.000	0.029	0.134
10 183.3GHz	0.052	-0.229	-0.006	0.027	0.137
11 183.3GHz	0.021	0.062	-0.011	***0.073***	0.617
12 19H	0.045	-0.142	-0.003	0.012	0.044
13 19V	0.046	-0.149	-0.002	0.012	0.044
14 22V	0.083	-0.225	0.001	0.006	0.020
15 37H	0.035	-0.132	0.001	0.027	0.112
16 37V	0.035	-0.128	0.002	0.028	0.111
17 92V	0.054	0.106	-0.004	***0.070***	0.325
18 92H	0.054	0.106	-0.004	***0.070***	0.317
19 63.3GHz	0.013	-0.059	-0.002	0.008	0.044
20 60.8GHz	0.007	0.033	-0.006	0.005	0.020
21 60.8GHz	0.030	-0.117	-0.024	0.022	0.131
22 60.8GHz	0.033	0.104	-0.066	***0.078***	0.423
23 60.8GHz	0.057	-0.191	-0.072	***0.129***	0.761
24 60.8GHz	0.046	-0.171	-0.016	***0.066***	0.484

[1]Only absolute values listed

Table 11. SSMI(S) brightness temperature statistics for RTTOV-6 (from Deblonde (2001)) and RTTOV-7 minus LbL values.Those channels with a significantly higher sdev for RTTOV-7 are bold and italicised.

SEVIRI Channel #	4 (3.9μm)	7 (8.7μm)	9 (10.8μm)	10 (12.0μm)
Zenith angle	**RTTOV-7 minus MODTRAN**			
Nadir	1.50(0.11) K	-0.14(0.16) K	-0.05(0.08) K	-0.04(0.08) K
60 deg	1.92(0.18) K	-0.01(0.22) K	0.03(0.11) K	0.11(0.11) K
Zenith angle	**RTTOV-7 minus RAD7**			
Nadir	1.70(0.16) K	0.26(0.18) K	0.05(0.08)K	0.07(0.11) K
60 deg	1.91(0.27) K	0.48(0.29) K	0.07(0.12) K	0.12(0.15) K

Table 12. Brightness temperature differences between RTTOV-7 and MODTRAN and RAD-7 RT models for 250 TIGR profiles over the sea. The latter 2 models have integrated the radiance over the spectral response. The mean bias and standard deviation in brackets are listed.

NOAA-14 HIRS/2 Channel Number	RTTOV-6				RTTOV-7			
	Bias (K)	Sdev (K)	Rms (K)	Max Value (K)	Bias (K)	Sdev (K)	Rms (K)	Max Value (K)
8	-0.156	0.107	0.189	0.942	-0.077	0.029	0.082	0.203
9	0.324	0.258	0.414	1.969	0.078	0.153	0.171	1.991
10	-0.055	0.207	0.214	1.001	0.112	0.072	0.133	0.458
11	0.396	0.517	0.652	1.841	0.113	0.103	0.153	0.526
12	0.184	0.858	0.878	5.252	-0.261	0.118	0.287	1.410
METEOSAT-7 MVIRI Channel number (wavelength)	RTTOV-6				RTTOV-7			
	Bias (K)	Sdev (K)	Rms (K)	Max Value (K)	Bias (K)	Sdev (K)	Rms (K)	Max Value (K)
1 (6.7μm)	-0.406	0.932	1.017	-6.045	-0.726	0.168	0.745	-2.044
2 (11μm)	-0.302	0.138	0.332	-1.183	-0.120	0.035	0.125	-0.331

Table 13. Statistics of the difference between fast model and SYNSATRAD generated radiances in HIRS and MVIRI channels for the 8987 profile independent set.

AVHRR Channel #	3b (3.7μm)	4 (11μm)	5 (12μm)	4-5 (11-12μm)
RTTOV-6 -MODTRAN	0.004(0.13) K	-0.106(0.11) K	-0.045(0.14) K	-0.061(0.06) K
RTTOV-7 -MODTRAN	0.015(0.12) K	-0.072(0.08) K	-0.002(0.10)K	-0.069(0.04) K

Table 14. AVHRR brightness temperature differences between RTTOV-7 and MODTRAN for 402 TIGR profiles over the sea. The mean bias and standard deviation in brackets are listed.

	AMSU-06		AMSU-10		AMSU-14		AMSU-18	
Model	std	bias	std	bias	std	bias	std	bias
RTTOV-5	0.04	-0.05	0.14	0.25	**1.35**	0.91	**0.60**	-0.16
RTTOV-6	0.04	-0.05	0.14	0.25	**1.35**	0.91	**0.28**	-0.38
RTTOV-7	0.04	-0.06	0.15	0.25	**1.36**	0.90	**0.35**	-0.39
OPTRAN	0.09	0.00	0.05	-0.04	**0.73**	-1.97	0.10	0.00
AER_OSS	0.06	0.13	0.04	0.03	0.09	0.14	0.14	-0.16
MIT	0.01	0.00	0.04	-0.04	0.08	-0.09	0.19	-0.40
RAYTHEON	**0.42**	-0.57	0.17	0.24	0.20	0.60	**0.50**	-0.07
AER_LBL	0.06	0.13	0.05	0.03	0.09	0.16	0.14	-0.15
MSCMWLBL	0.03	0.05	0.03	0.04	0.20	0.51	**0.32**	-0.36
ATM	0.19	0.46	0.07	0.08	0.11	0.23	0.24	-0.28

Table 15. Brightness temperature standard deviation and bias of various models against the CIMSS MWLBL model for 4 AMSU channels. St. devs above 0.25K are in bold (adapted from Garand et. al. 2001).

	RTTOV-6												
Garand Profile #	T H-2	T H-5	O_3 H-5	T H-9	H_2O H-9	O_3 H-9	T H-10	H_2O H-10	T H-11	H_2O H-11	T H-12	H_2O H-12	T H-15
6	2.3	4.1	23.4	17.8	7.9	11.2	8.7	7.1	9.5	12.2	7.7	17.2	2.7
18	2.4	2.7	22.0	27.0	12.2	23.2	5.8	18.9	4.7	16.5	12.2	20.2	2.7
19	2.7	4.5	-----	8.7	-----	19.8	6.3	-----	12.6	10.0	13.5	16.6	3.4
30	2.4	4.2	26.8	10.4	3.1	25.0	8.8	11.5	7.8	17.0	18.5	13.4	2.7
31	2.7	3.9	-----	11.2	-----	9.7	-----	-----	9.5	15.8	10.2	18.0	4.4
	RTTOV-7												
Garand Profile #	T H-2	T H-5	O_3 H-5	T H-9	H_2O H-9	O_3 H-9	T H-10	H_2O H-10	T H-11	H_2O H-11	T H-12	H_2O H-12	T H-15
6	2.7	2.5	15.2	7.2	3.1	4.6	6.5	3.0	3.1	3.6	1.5	2.0	2.3
18	2.7	2.7	8.4	8.7	1.6	5.2	3.9	3.7	2.1	3.2	3.8	4.2	2.3
19	2.9	2.4	-----	2.7	-----	5.9	6.4	-----	3.6	8.7	2.9	4.6	3.2
30	2.7	2.3	8.3	4.3	1.7	5.8	2.7	2.8	3.0	6.4	7.0	6.8	2.1
31	3.1	2.5	-----	4.6	-----	9.8	-----	-----	3.21	7.5	2.2	6.0	4.3

Table 16. Quality of fit measure M (no units) for temperature (T), ozone (O3) or water vapour (H2O) Jacobians for 5 independent atmospheric profiles in selected HIRS channels. Reference line-by-line Jacobians were obtained using GENLN2.

RTTOV-6					
Garand Profile #	T A-6	T A-10	T A-14	T A-18	H_2O A-18
6	0.6	2.1	29.1	2.8	1.9
18	0.7	2.4	28.4	3.2	1.9
19	0.7	2.0	28.4	2.0	1.1
30	0.6	2.4	28.6	3.3	1.6
31	0.8	2.4	28.9	2.0	2.5
RTTOV-7					
Garand Profile #	T A-6	T A-10	T A-14	T A-18	H_2O A-18
6	0.6	2.2	28.5	2.9	1.8
18	0.8	2.4	27.9	3.3	1.9
19	0.7	2.0	28.2	2.1	***1.7***
30	0.7	2.4	28.2	3.2	1.4
31	0.8	2.5	28.7	1.9	***4.6***

Table 17. Quality of fit measure M (no units) for temperature (T) or water vapour (H_2O) Jacobians for 5 independent atmospheric profiles in selected AMSU channels. Reference line-by-line Jacobians were obtained using MWLBL (see Garand et. al. 2001 for more details). The high values for AMSU-14 are due to the MWLBL not including the Zeeman effect.

	RTTOV-6					
Profile	T H-9	O_3 H-9	T H-12	H_2O H-12	T M-1	H_2O M-1
All	19.531	14.413	17.395	30.727	17.237	31.204
Mid/High-Latitude	22.365	11.332	16.268	24.070	16.193	24.161
Tropical	16.212	18.021	18.715	38.521	18.461	39.448
	RTTOV-7					
Profile	T H-9	O_3 H-9	T H-12	H_2O H-12	T M-1	H_2O M-1
All	12.034	6.312	2.578	7.315	4.302	7.493
Mid/High-Latitude	15.806	5.918	2.708	7.703	4.341	7.837
Tropical	7.617	6.772	2.426	6.861	4.256	7.090

Table 18. Quality of fit measure M (no units) for temperature (T), water vapour (H_2O) or ozone (O_3) Jacobians in channels HIRS-9, HIRS-12 and METEOSAT water vapour channel. Reference line-by-line Jacobians were obtained using SYNSATRAD.

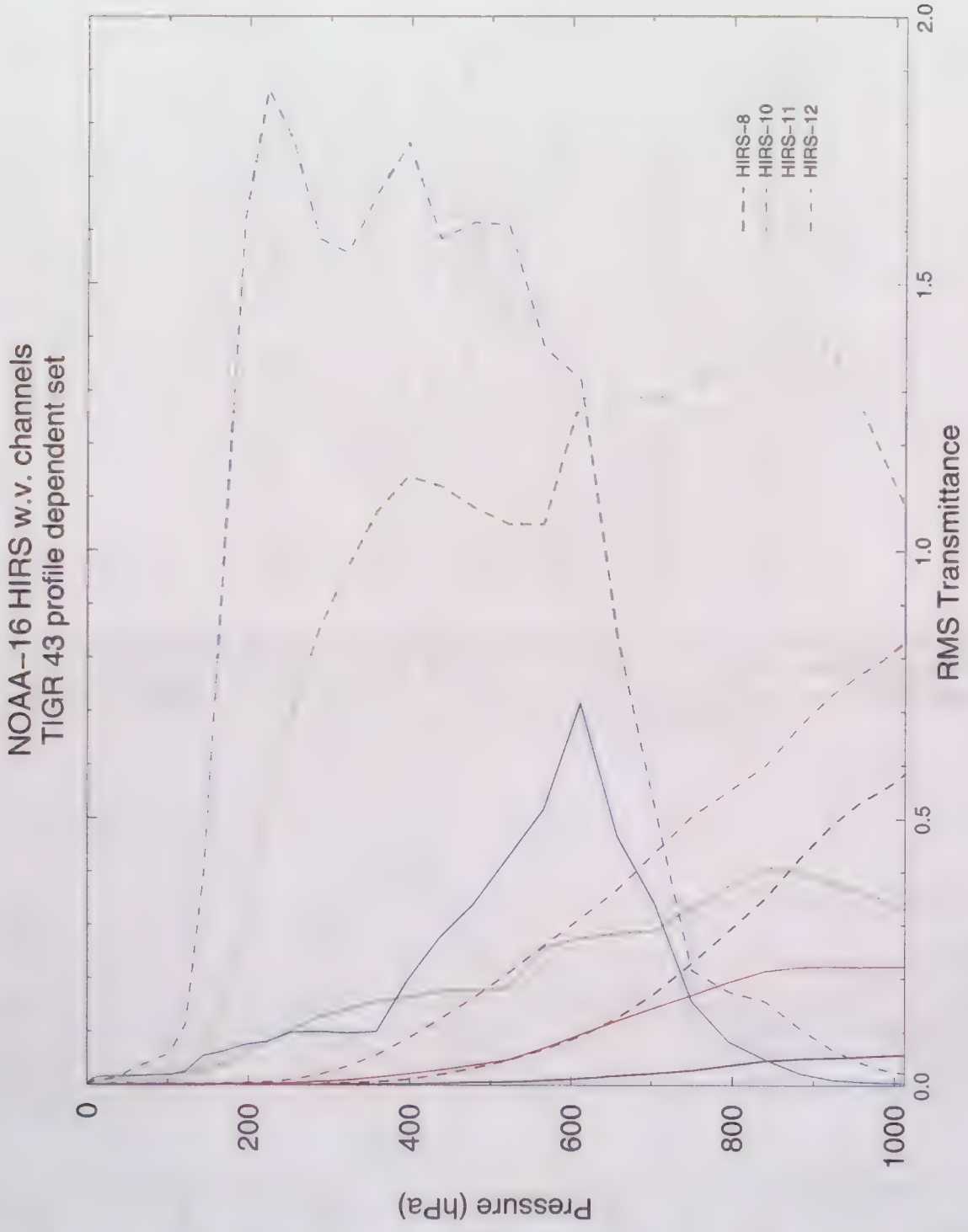

Figure 1a RMS of RTTOV-6 (dashed lines) and RTTOV-7 (solid lines) for NOAA-16 HIRS transmittance differences (X100) from GENLN2 LbL model for 43 TIGR profiles and 5 viewing angles.

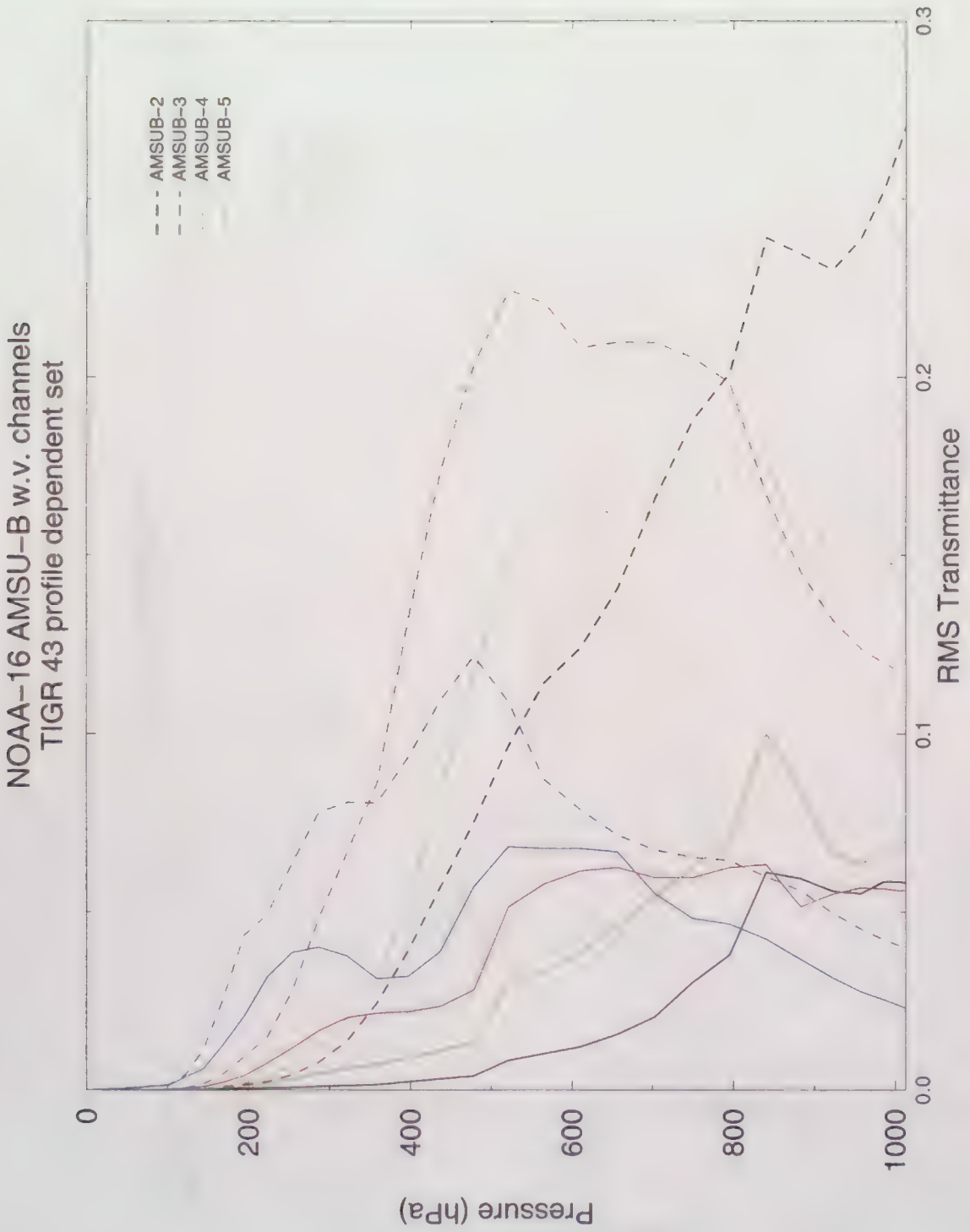

Figure 1b RMS of RTTOV-6 (dashed lines) and RTTOV-7 (solid lines) for NOAA-16 AMSU-B transmittance differences (X100) from MPM LbL model for 43 TIGR profiles and 5 viewing angles.

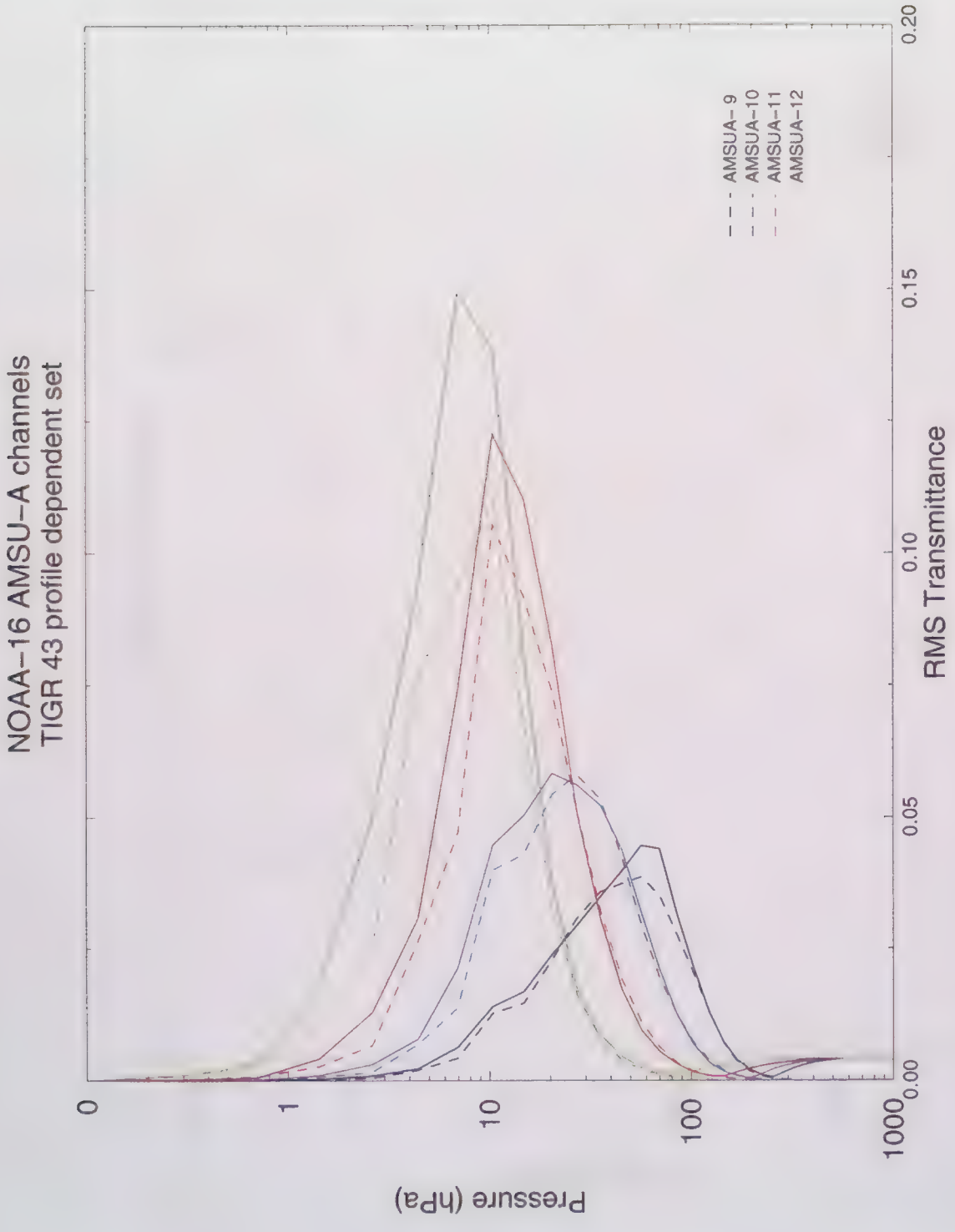

Figure 1c RMS of RTTOV-6 (dashed lines) and RTTOV-7 (solid lines) for NOAA-16 AMSU-A transmittance differences (X100) from MPM LbL model for 43 TIGR profiles and 5 viewing angles.

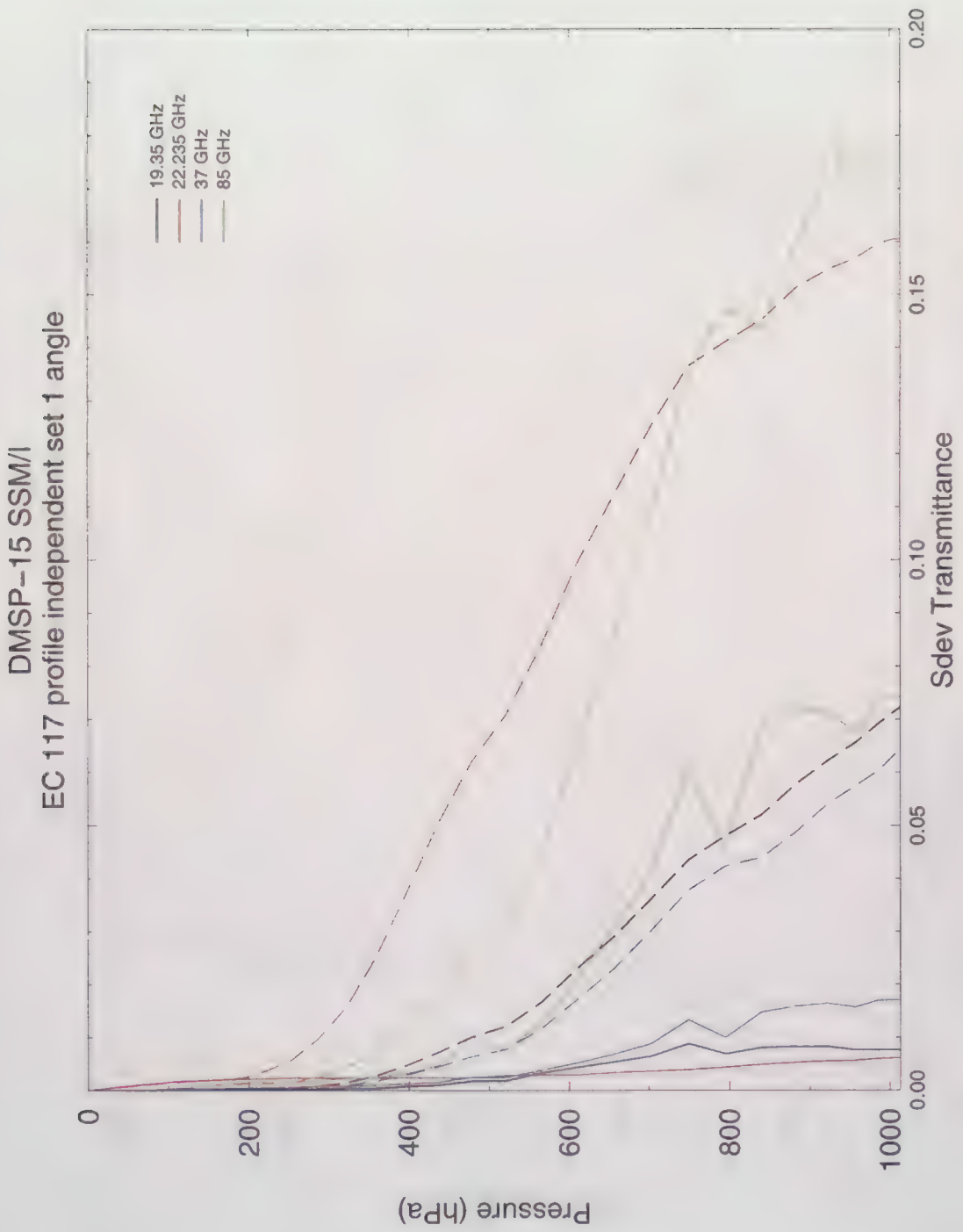

Fig 2a RMS of RTTOV-6 (dashed line) and RTTOV-7 (solid line) SSM/I transmittance differences (X100) from MPM LbL model.

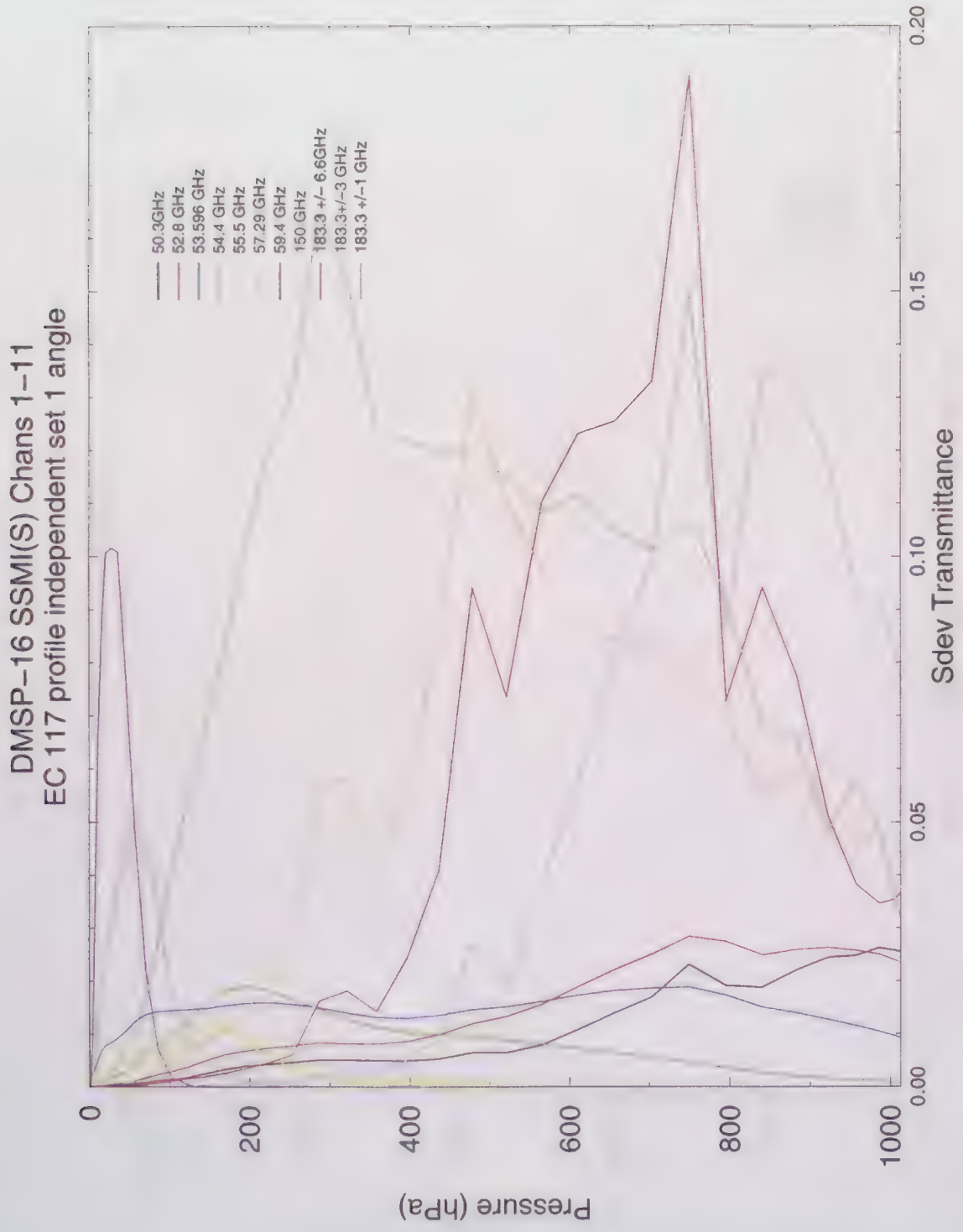

Fig 2b RMS of RTTOV-7 SSMI(S) transmittance differences (X100) from MPM LbL model

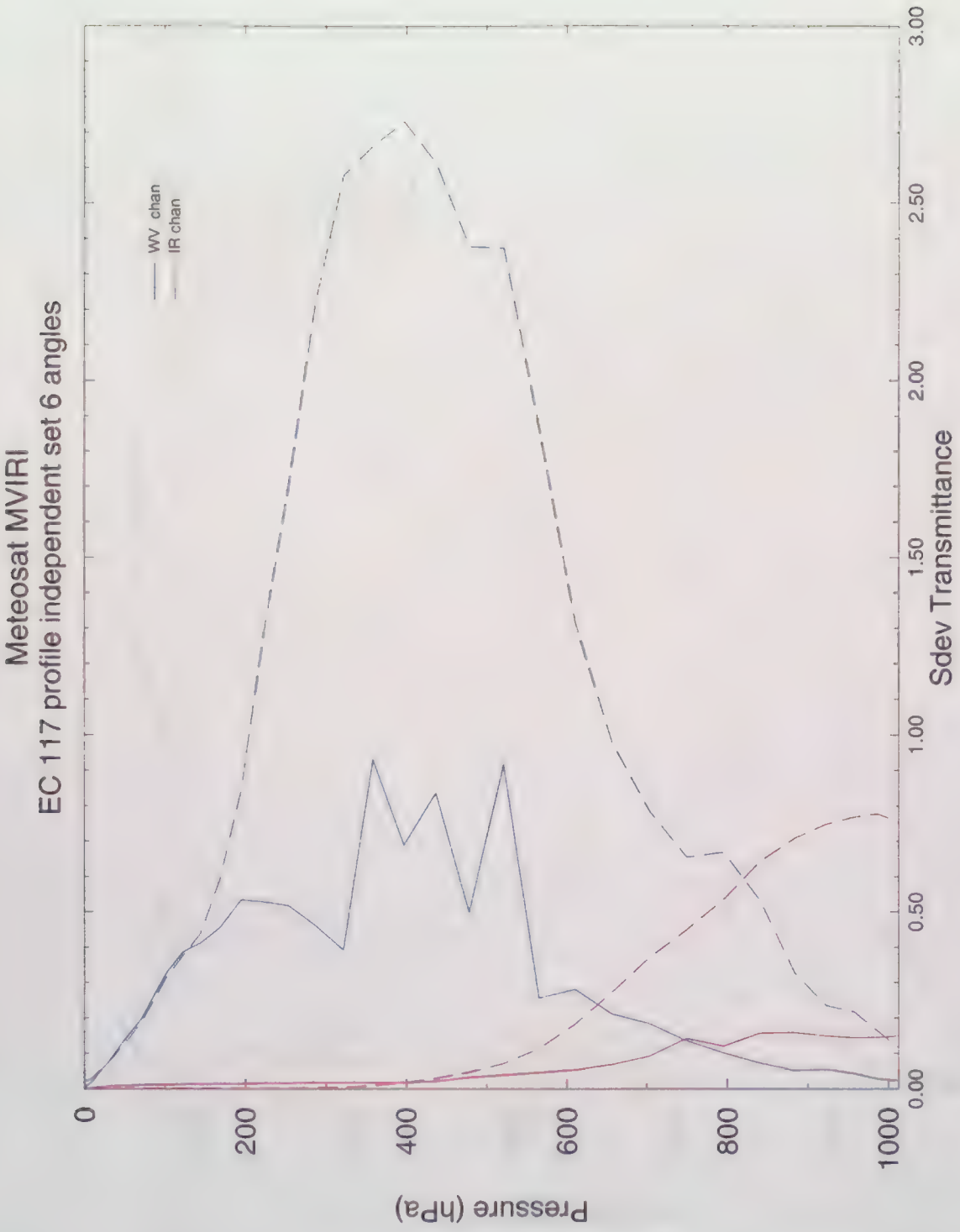

Fig 3a RMS of RTTOV-6 (dashed lines) and RTTOV-7 (solid lines) MVIRI transmittance differences (X100) from GENLN2 LbL model

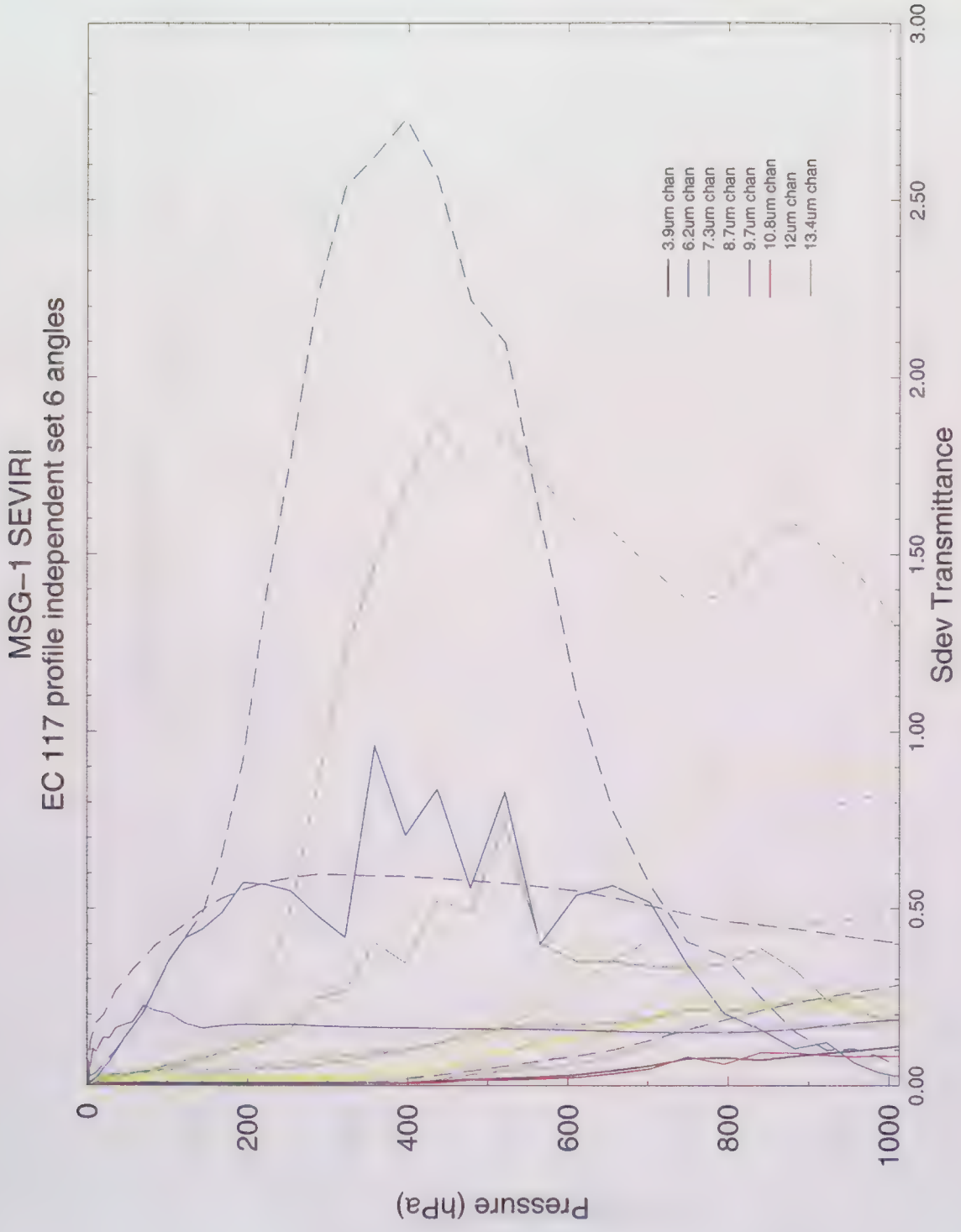

Fig 3b RMS of RTTOV-6 (dashed lines) and RTTOV-7 (solid lines) for SEVIRI transmittance differences (X100) from GENLN2 LbL model

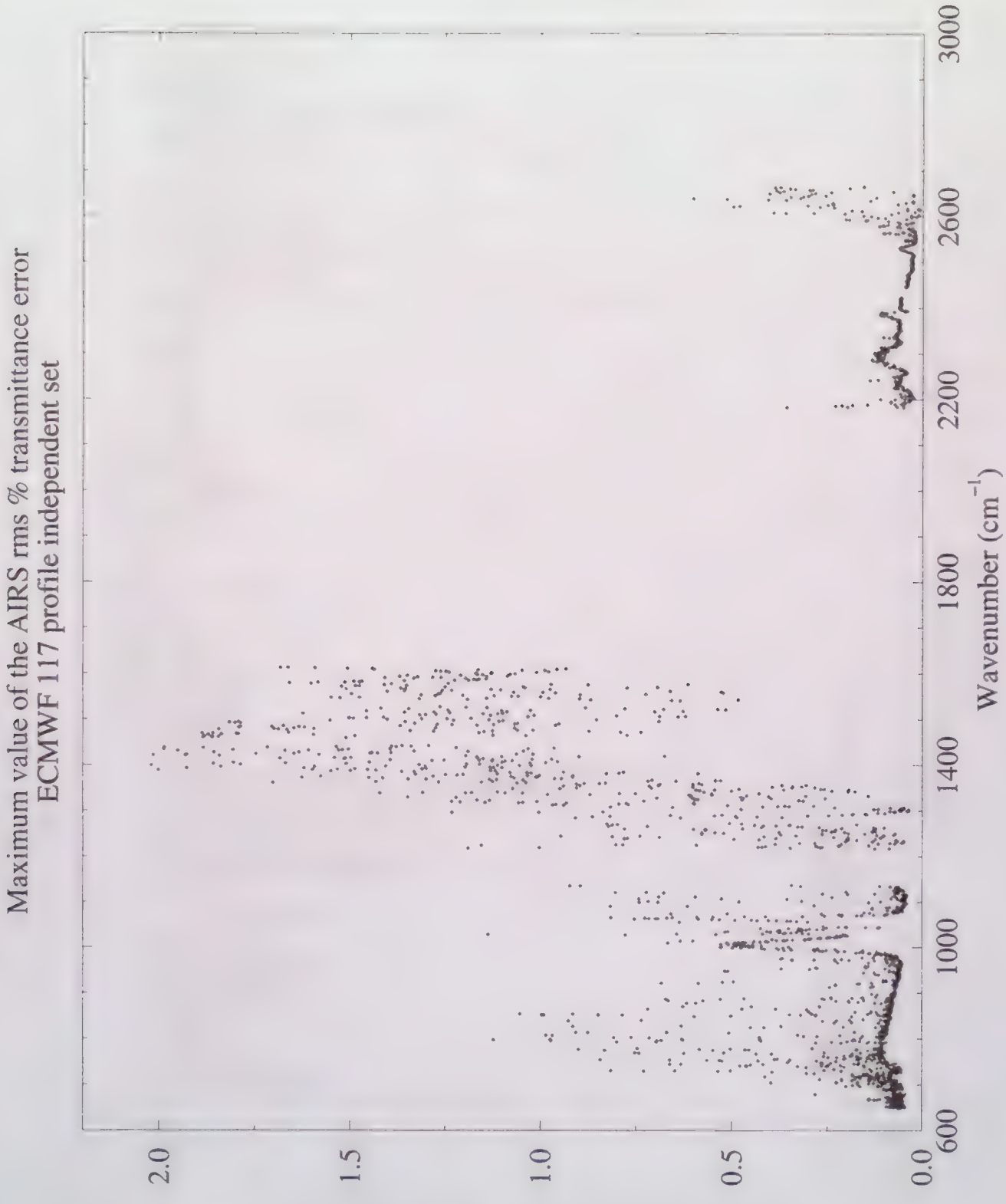

Figure 4 Maximum value of rms transmittance difference (X100) between fast model and GENLN2 layer to top of atmosphere transmittances for AIRS for 117 independent profiles and 6 viewing angles.

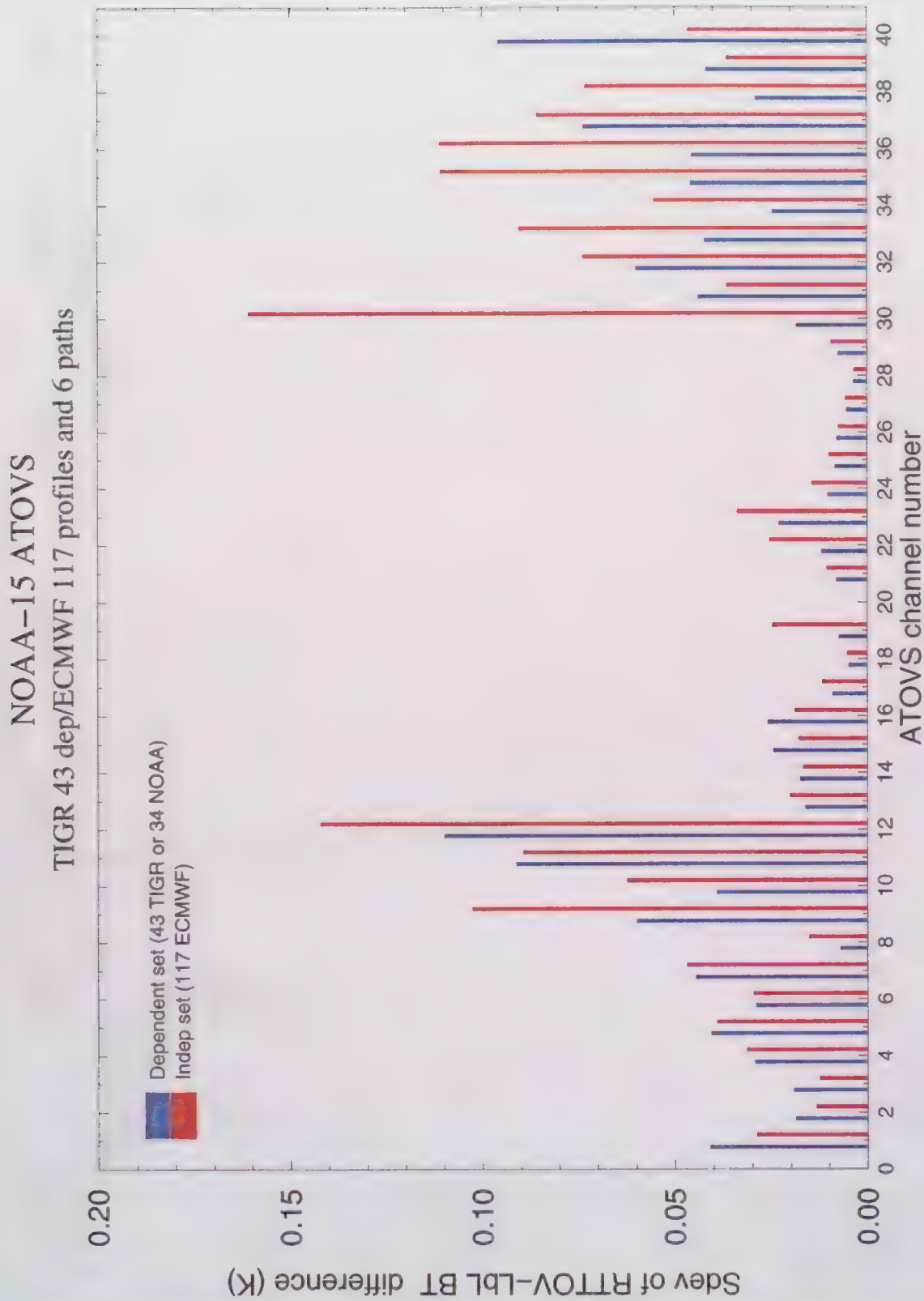

Figure 5. Comparison of standard deviation of brightness temperature differences for 6 viewing angles for dependent and independent profile sets for NOAA-15 ATOVS (note that for HIRS channel 9 the dependent set is the 34 NOAA ozone profiles and all other channels it is the 43 TIGR water vapour profiles). Channels 1-19 = HIRS; 21-35=AMSU-A; 36-40=AMSU-B.

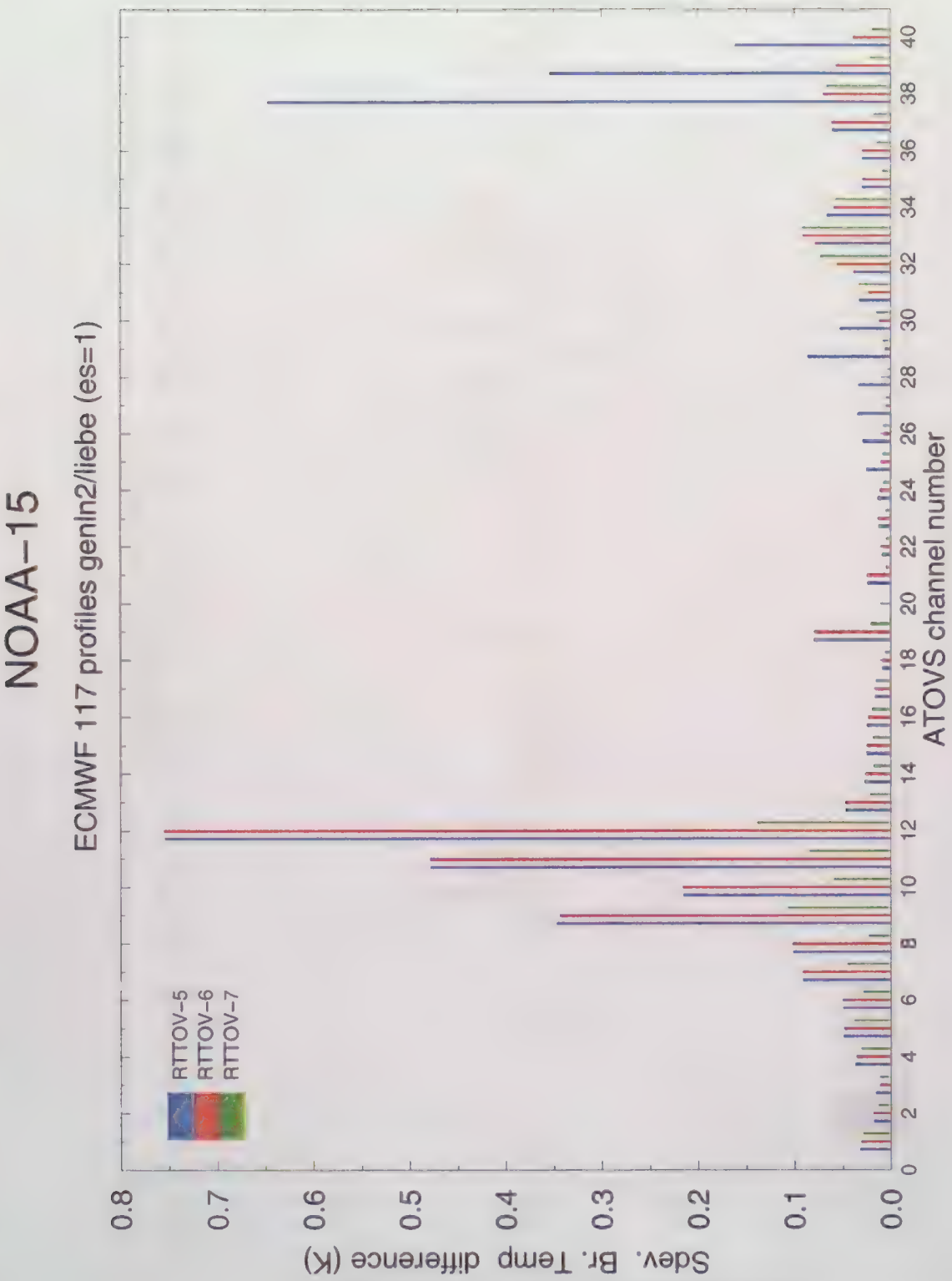

Figure 6a. Standard deviation of RTTOV-5, 6 and 7 top of atmosphere brightness temperature differences from LbL for the 117 independent profile set and 5 viewing angles for NOAA-15 ATOVS. Channels 1-19 = HIRS; 21-35=AMSU-A; 36-40=AMSU-B. A surface emissivity of 1 is assumed for all channels.

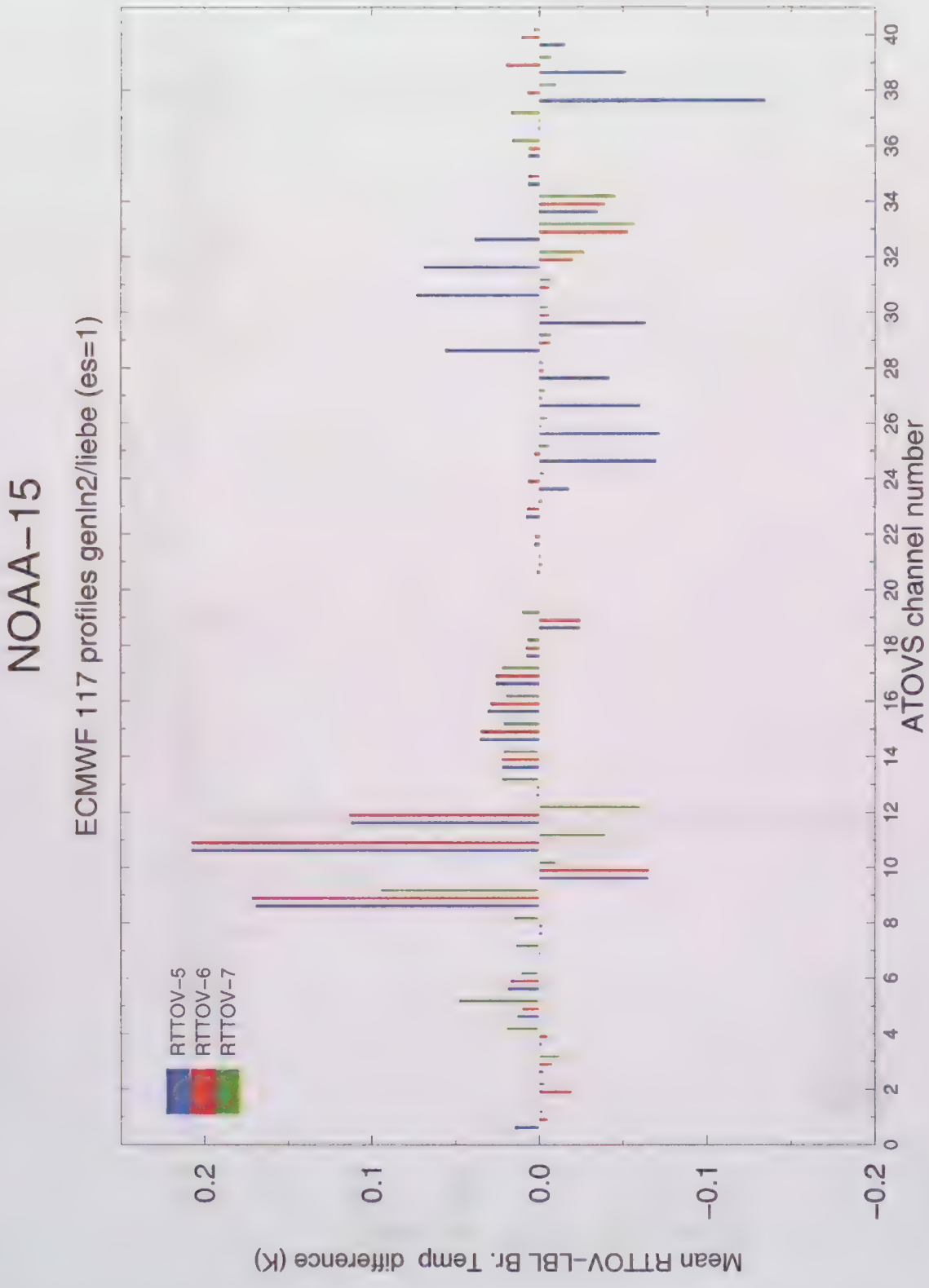

Figure 6b. Mean differences of RTTOV-5, 6 and 7 top of atmosphere brightness temperatures from LbL for the 117 independent profile set and 5 viewing angles for NOAA-15 ATOVS. Channels 1-19 = HIRS; 21-35=AMSU-A; 36-40=AMSU-B. A surface emissivity of 1 is assumed for all channels.

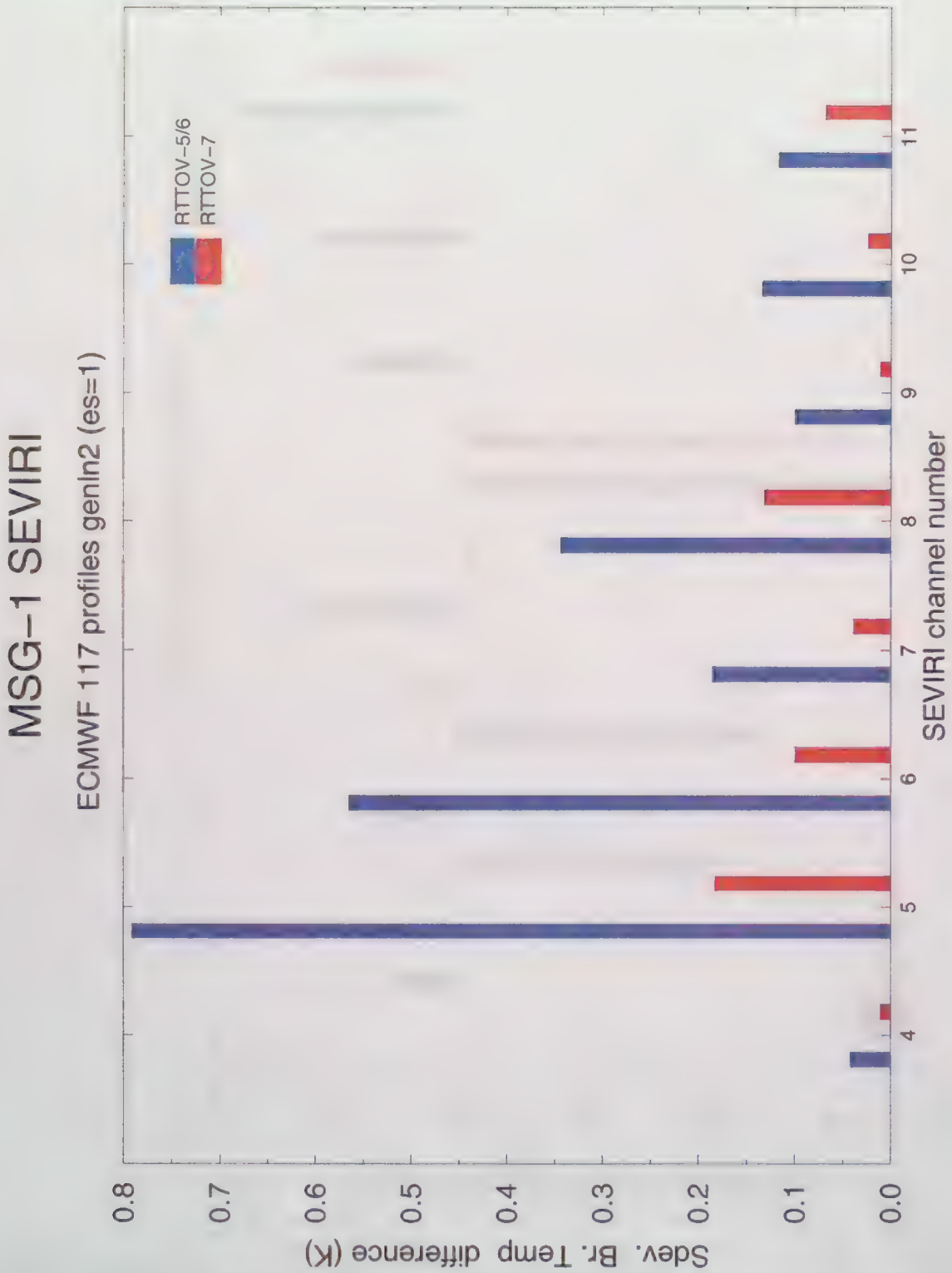

Figure 7a. Standard deviation of RTTOV-6 and 7 top of atmosphere brightness temperature differences from LbL for the 117 independent profile set and 6 viewing angles for MSG-1 SEVIRI.

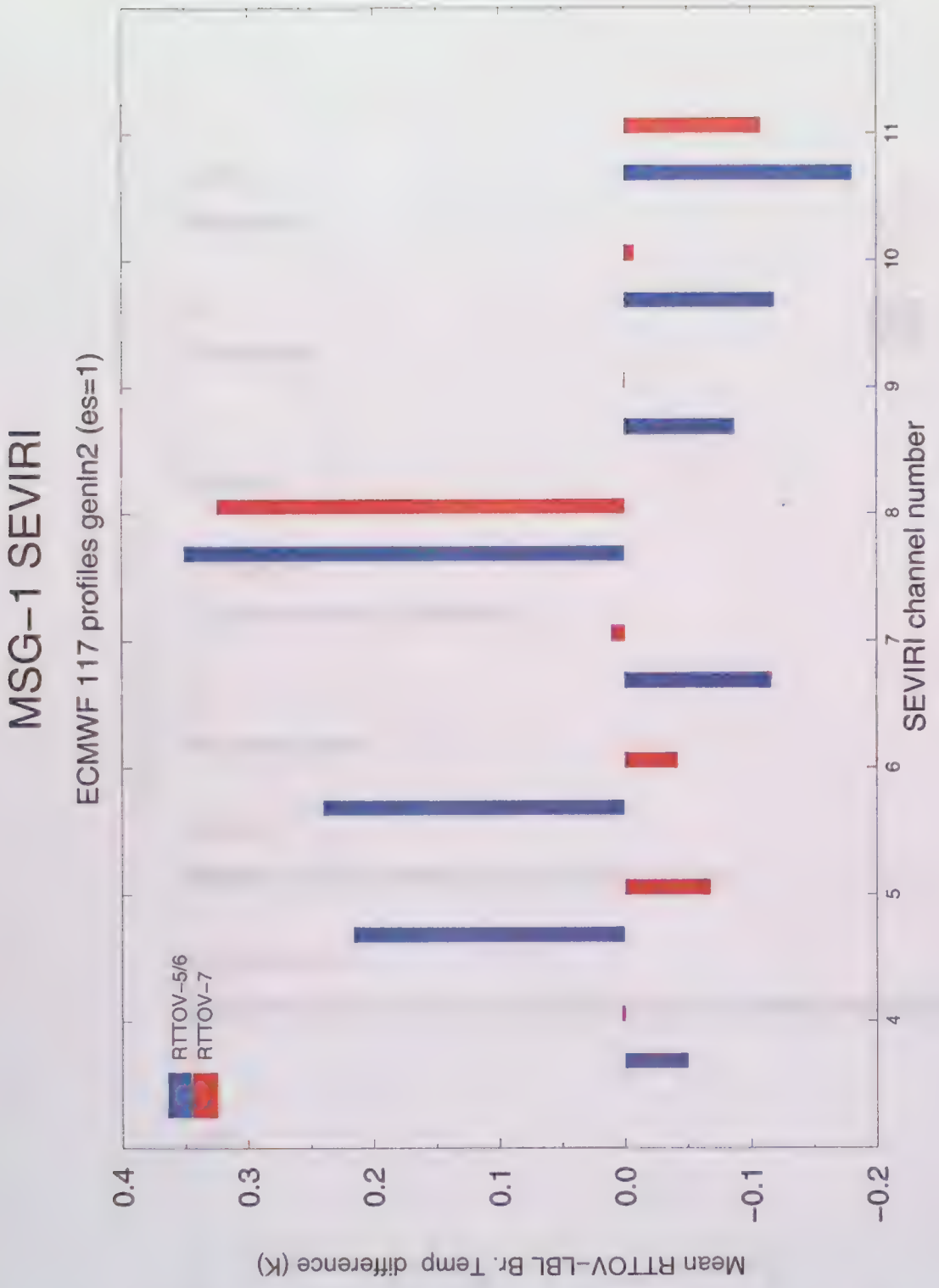

Figure 7b. Mean differences of RTTOV-6 and 7 top of atmosphere brightness temperatures from LbL for the 117 independent profile set and 6 viewing angles for MSG-1 SEVIRI.

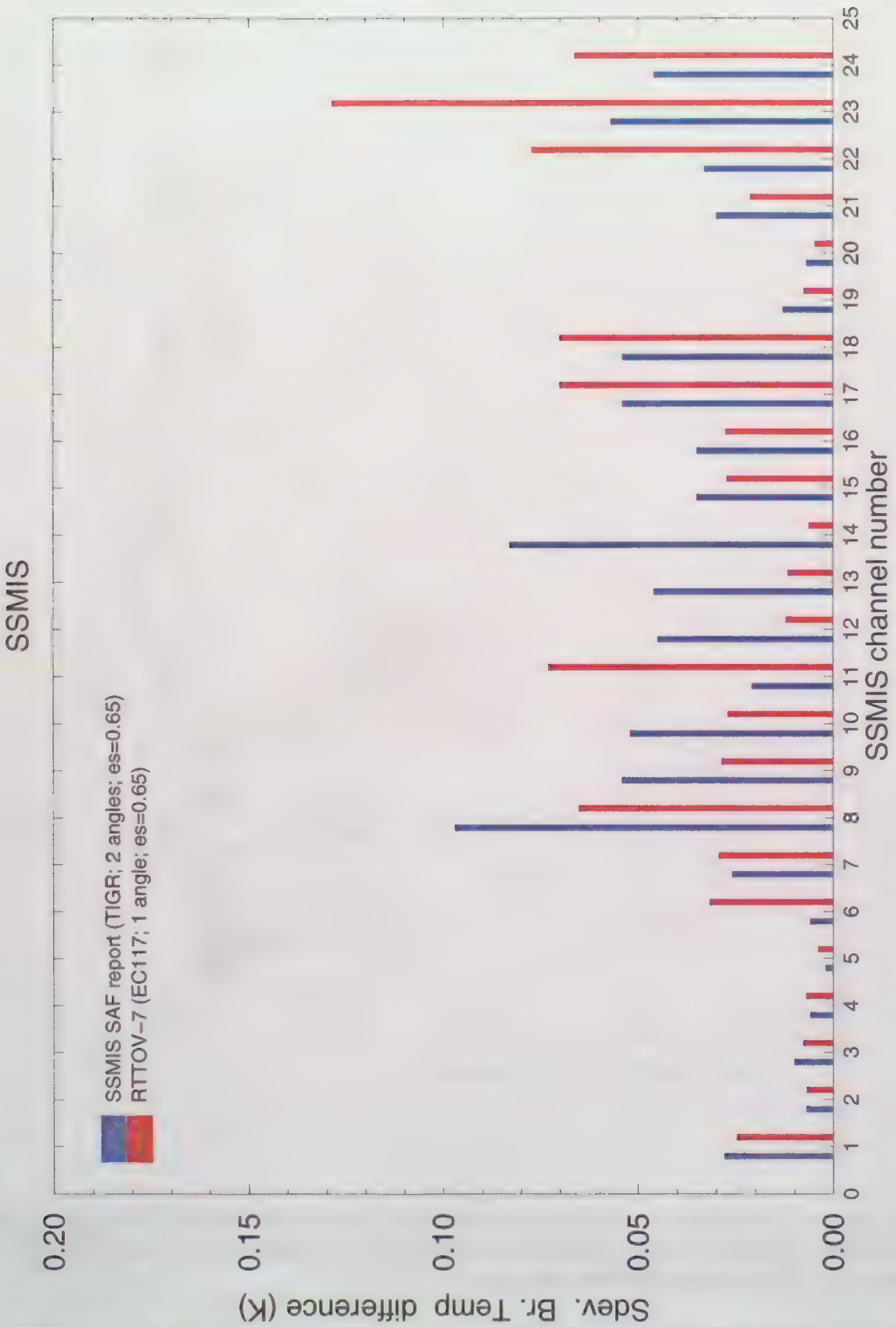

Figure 8. Standard deviation of RTTOV-6 and 7 top of atmosphere brightness temperature differences from LbL for the 117 independent profile set and 1 viewing angle for DMSP F-16 SSMI(S).

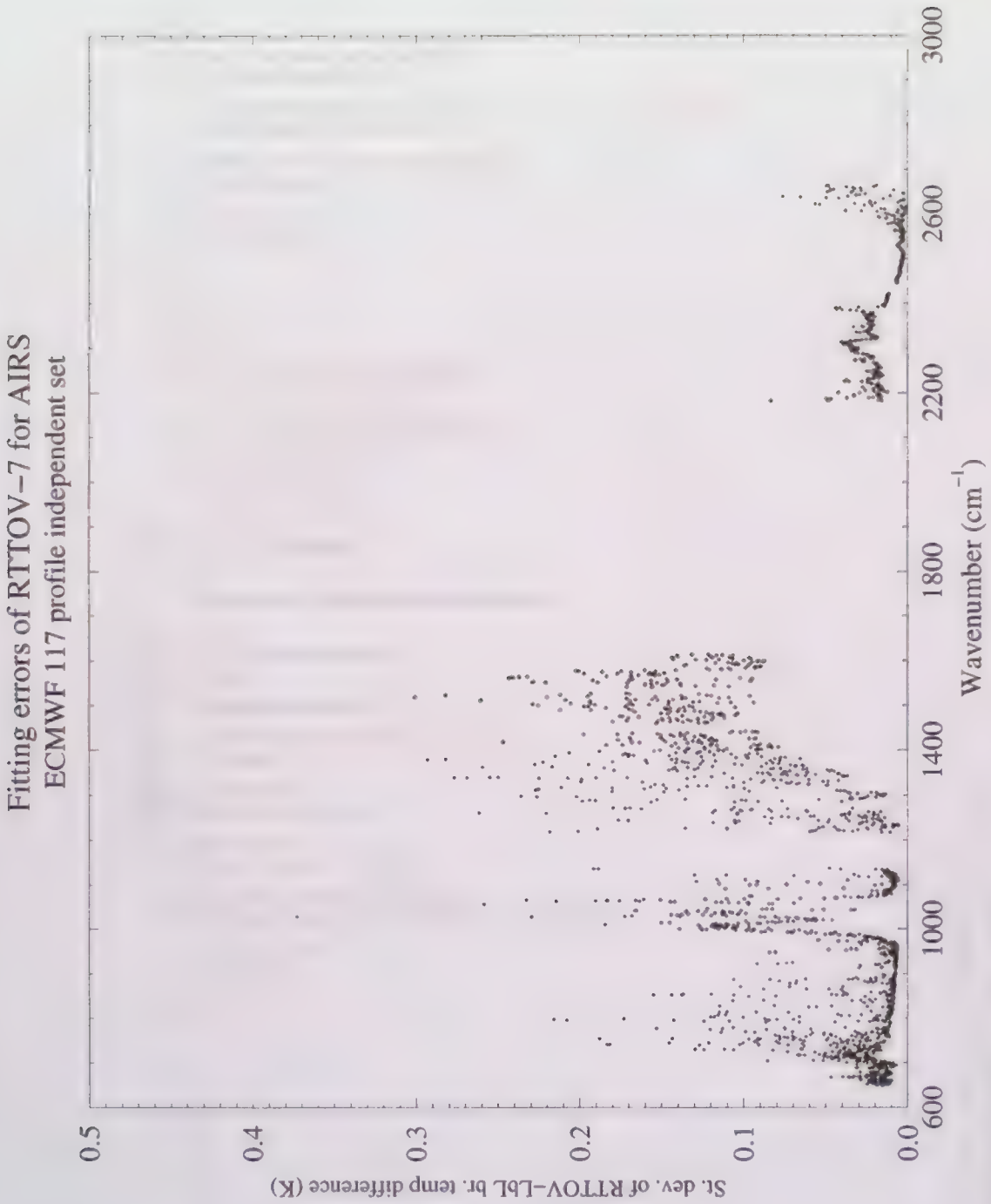

Figure 9a. Standard deviation of the difference between RTTOV-7 and GENLN2 computed AIRS top of atmosphere brightness temperatures for 117 ECMWF profile set and 6 viewing angles. A surface emissivity of 1 is assumed for all channels.

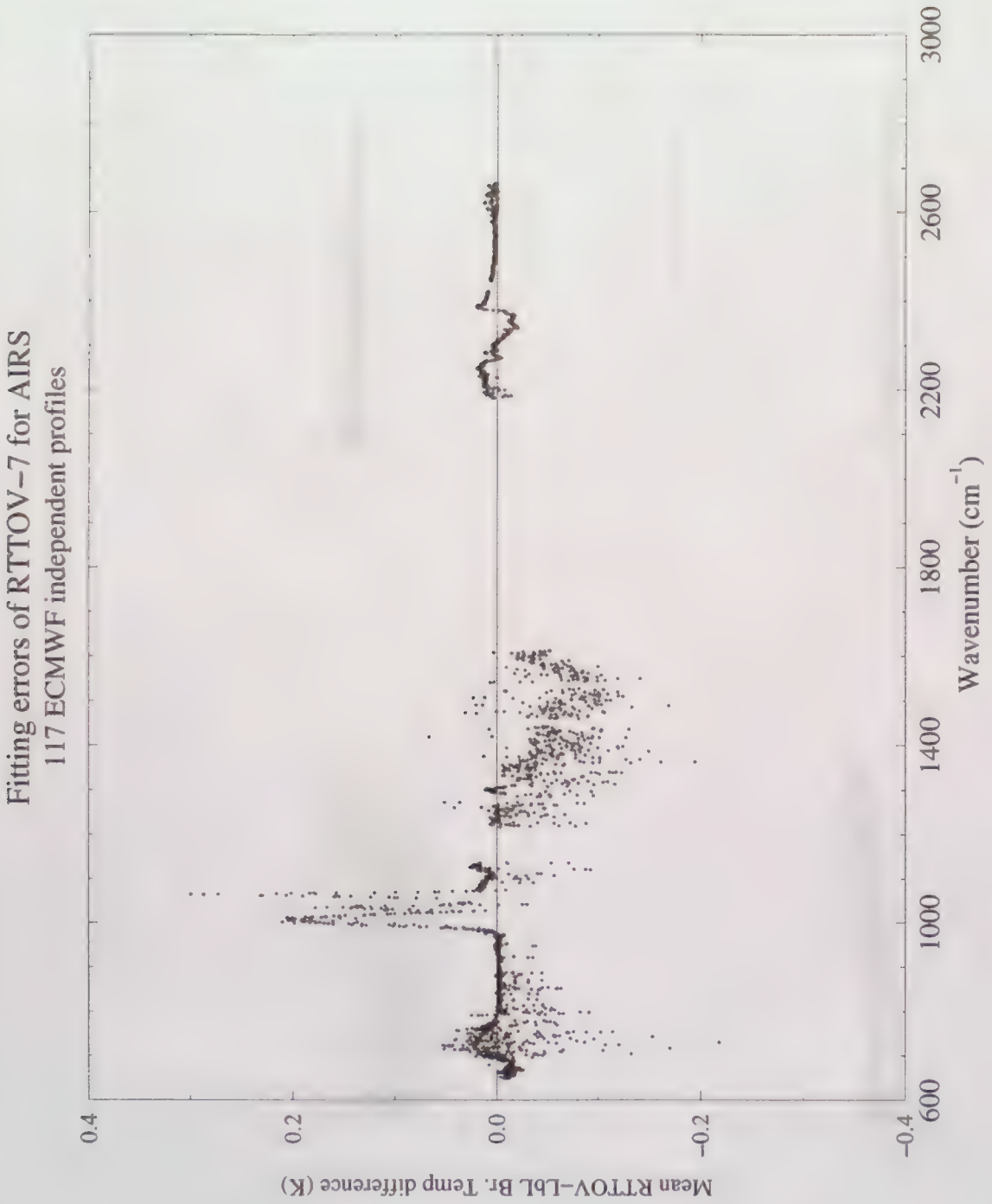

Figure 9b. Mean difference between RTTOV-7 and GENLN2 computed AIRS top of atmosphere brightness temperatures for 117 ECMWF profile set and 6 viewing angles.

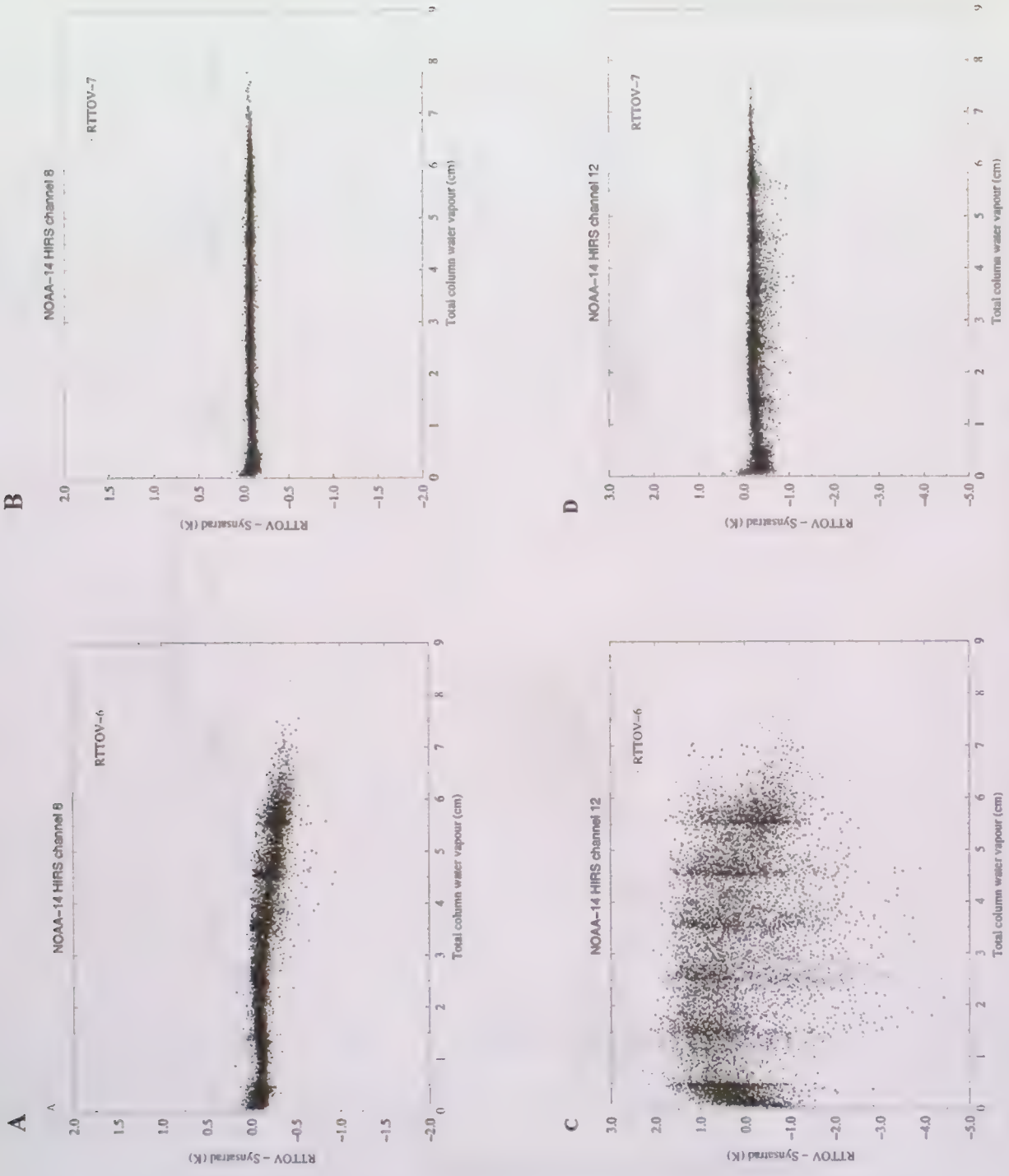

Figure 10. Difference between RTTOV-6 (left panels) and RTTOV-7 (right panels) with SYNSATRAD computed brightness temperatures for 8987 profiles for HIRS channels 8 and 12 of NOAA-14.

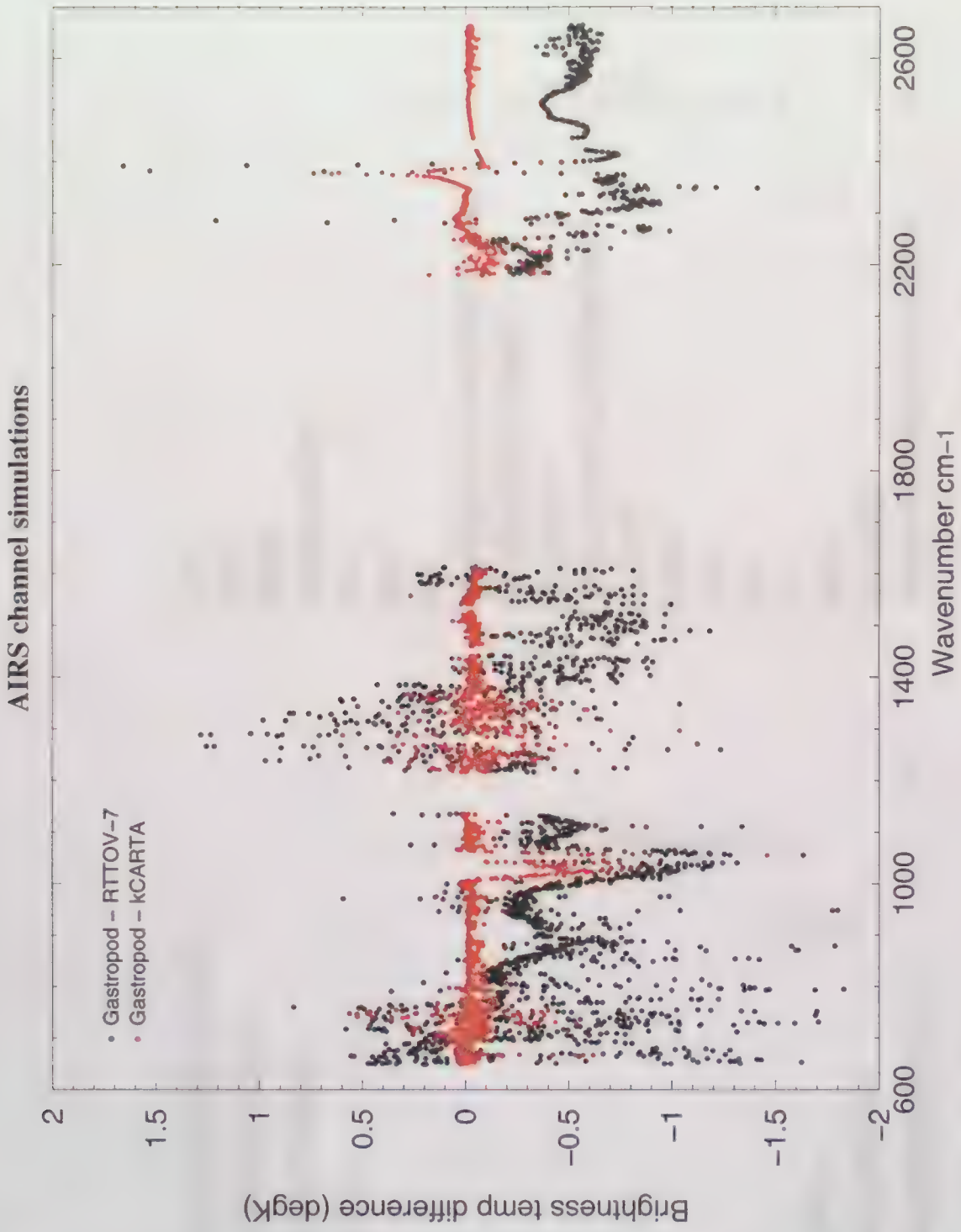

Figure 11. AIRS brightness temperature difference for Gastropod minus RTTOV-7 for the first ECMWF profile of the 117 set.

A

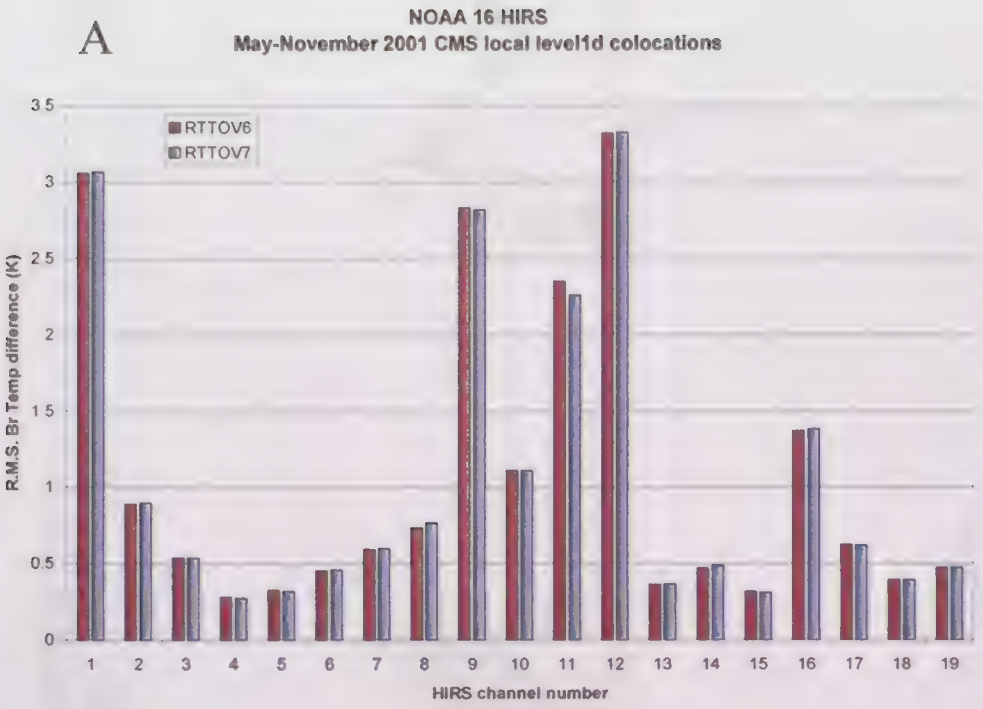

B

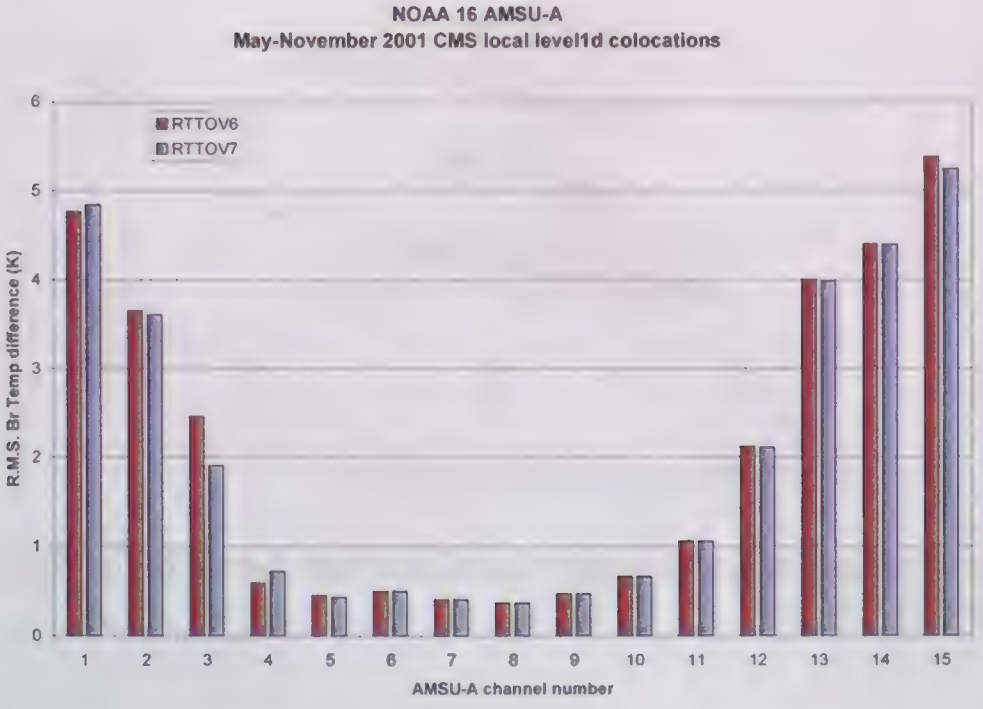

Figure 12 continued on next page

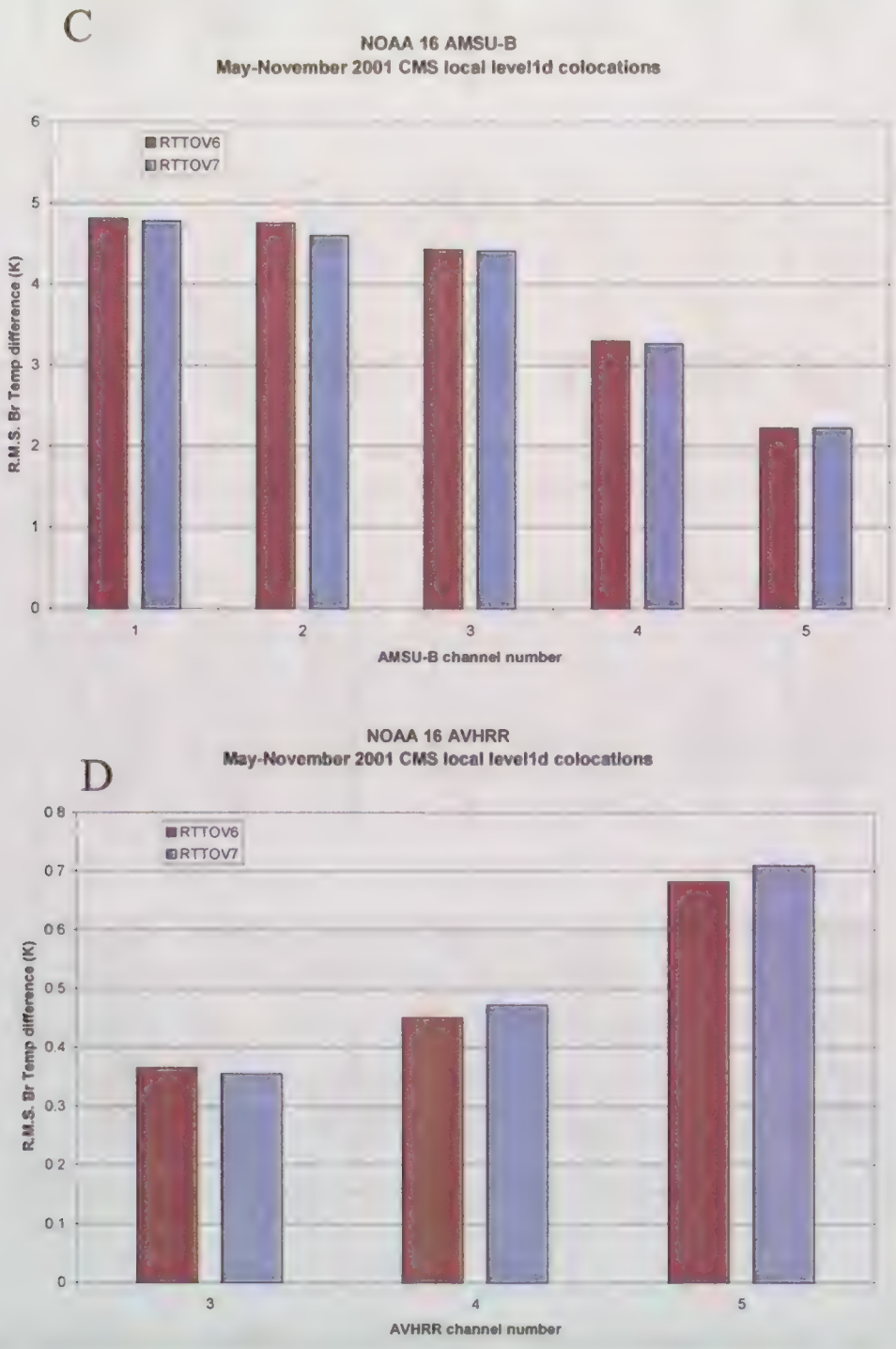

Figure 12. Statistics of rms differences of observed minus simulated brightness temperatures from RTTOV-6 and 7 for HIRS (A), AMSU-A (B), AMSU-B (C) and AVHRR (D) clear sky radiances for the period May-November 2001 over the Lannion reception area.

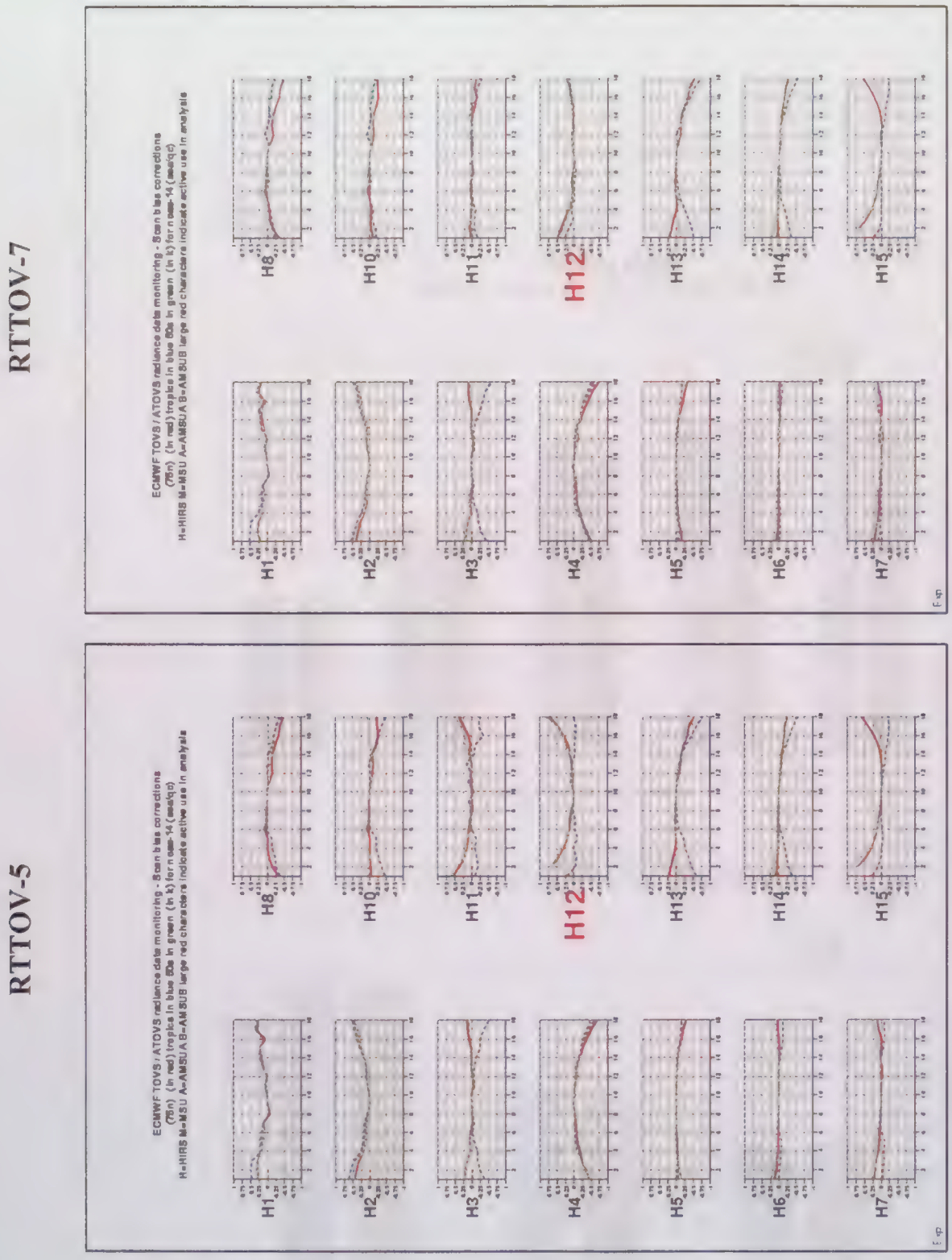

FIgure 13. Plots of observed minus simulated HIRS radiances plotted as a function of HIRS scan angle for different latitude bands (red 75N; blue tropics; green 50S) for RTTOV-5 and RTTOV-7 using ECMWF 6 hour forecast fields.

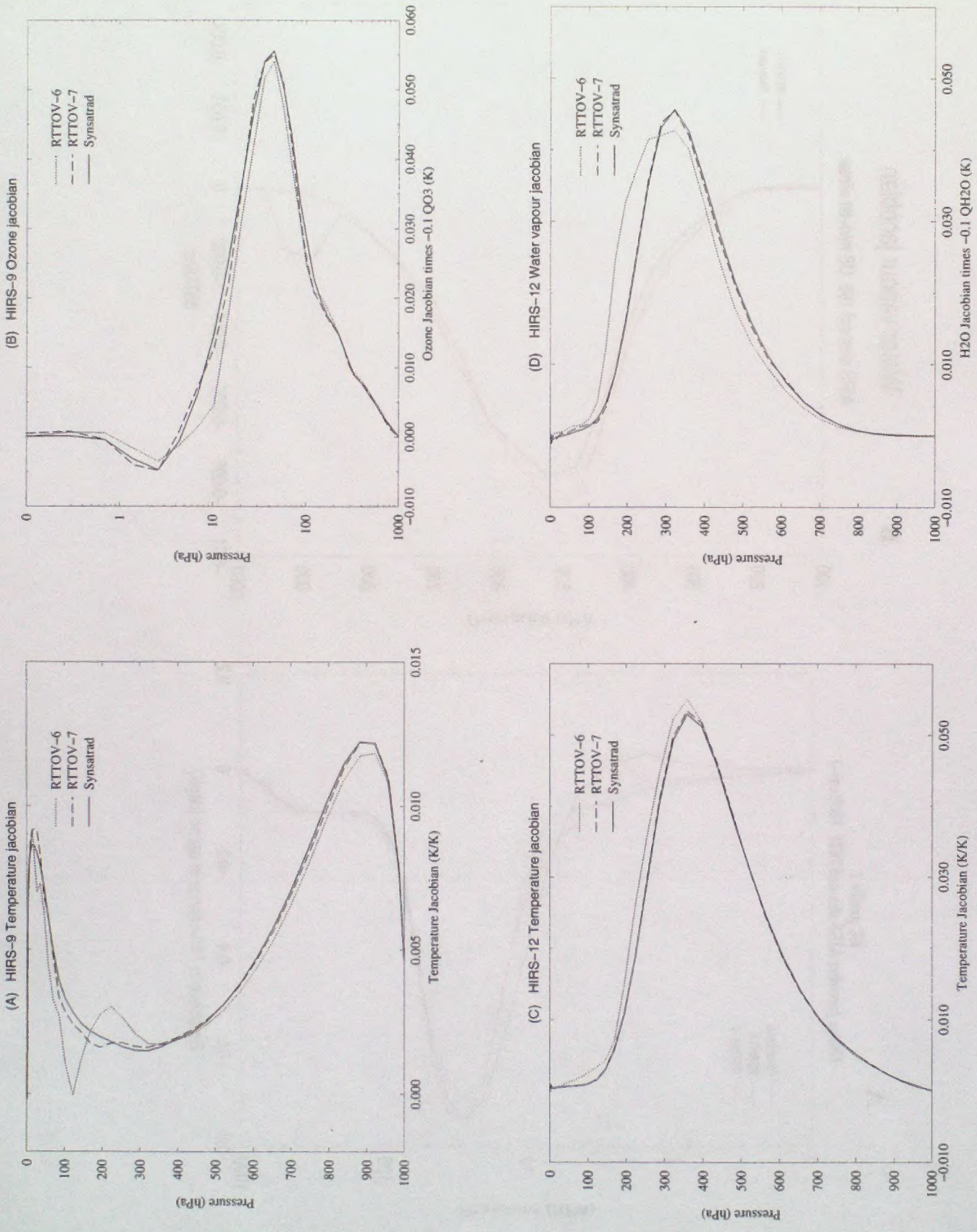

Figure 14. Mean Jacobians computed by RTTOV-6 and RTTOV-7 for HIRS channels 9 and 12 compared with SYNSATRAD finite difference Jacobians for 8978 profiles.

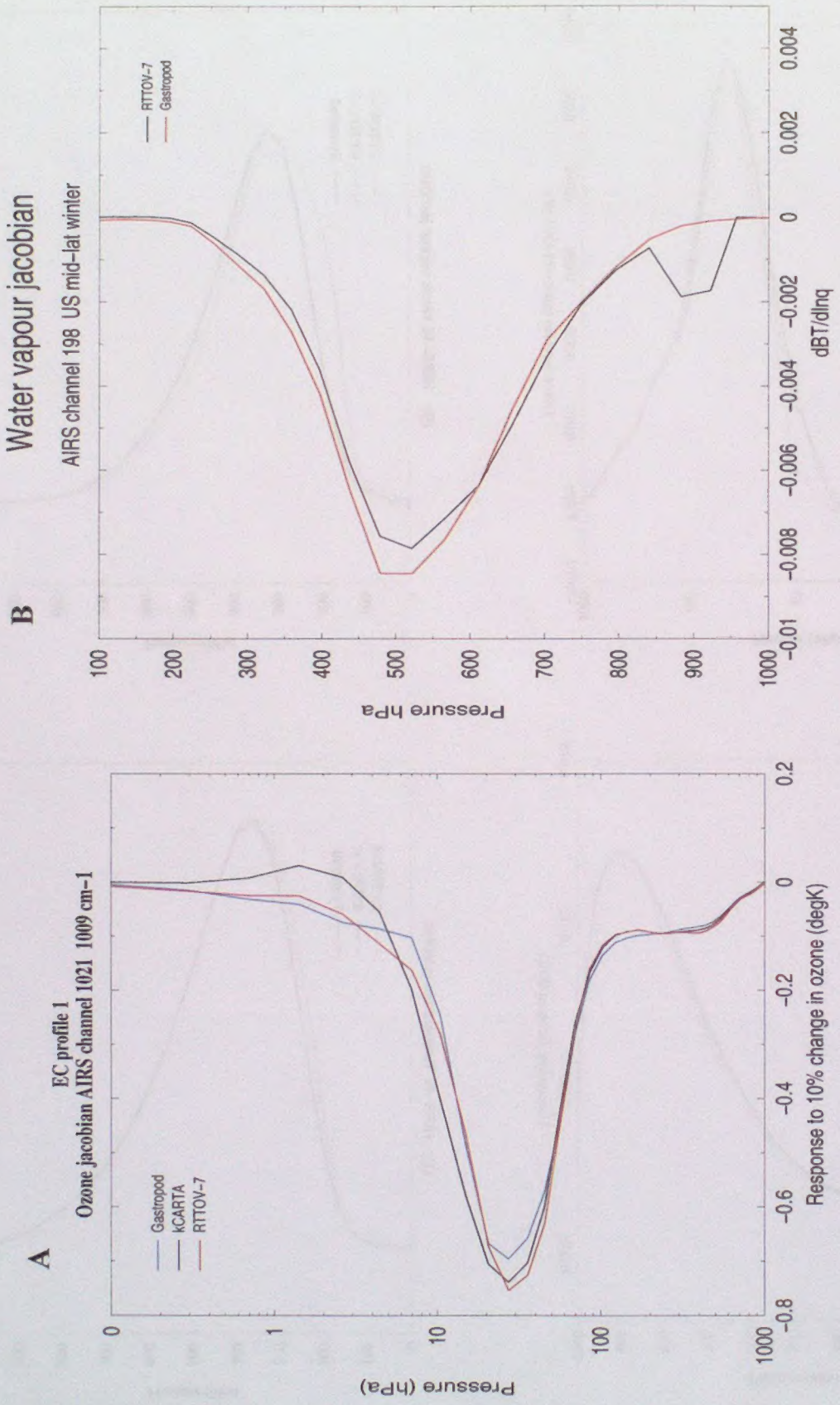

Figure 15. Jacobians for AIRS channels. Panel A shows the ozone Jacobians for AIRS channel 1021 computed by RTTOV-7, Gastropod and kCARTA. Panel B shows the water vapour Jacobian for AIRS channel 198 computed by RTTOV-7 and Gastropod.

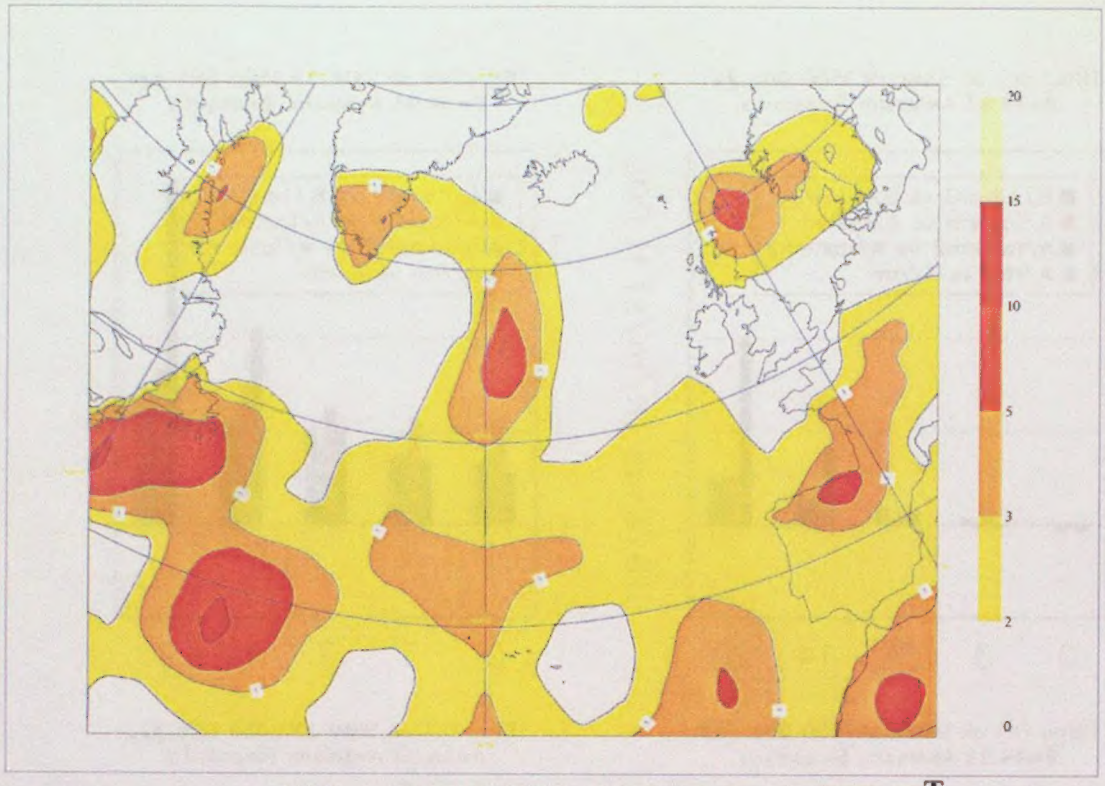

(A) RTTOV-5 HIRS-12 HBH^T

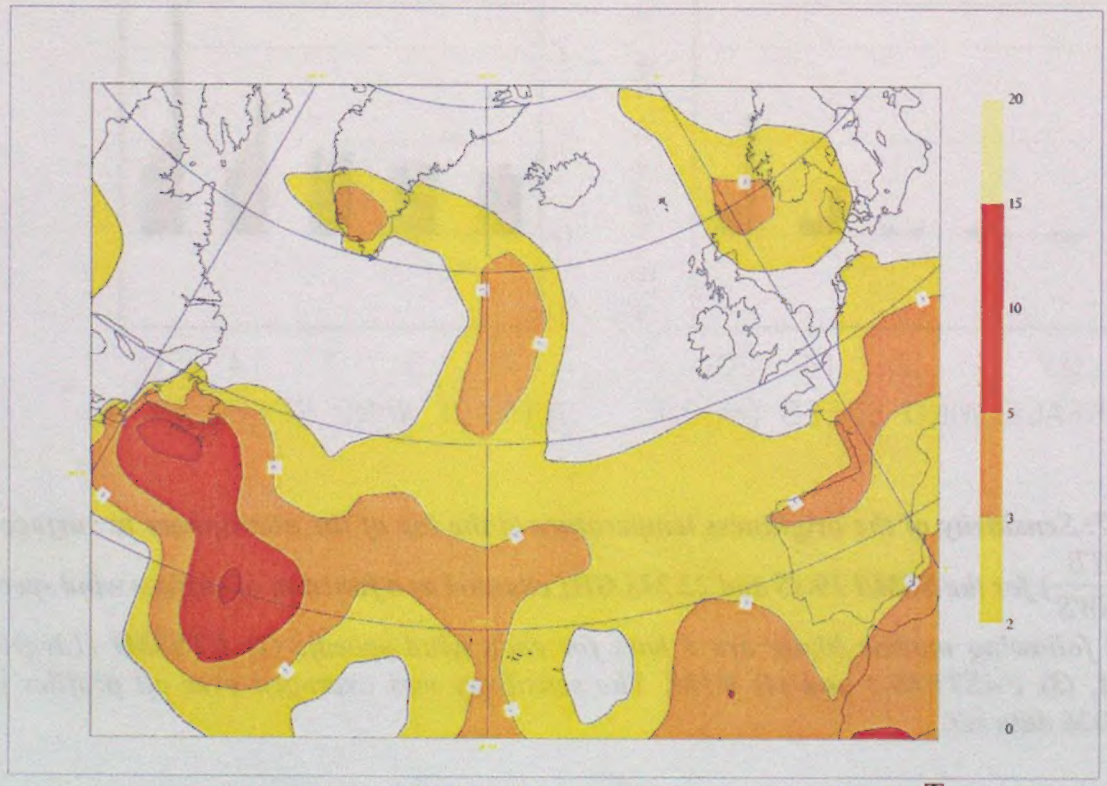

(B) RTTOV-7 HIRS-12 HBH^T

Figure 16 Plots of the ECMWF background error transformed into HIRS-12 brightness temperatures for RTTOV-5 (A) and RTTOV-7 (B) for 1 Sep 2001

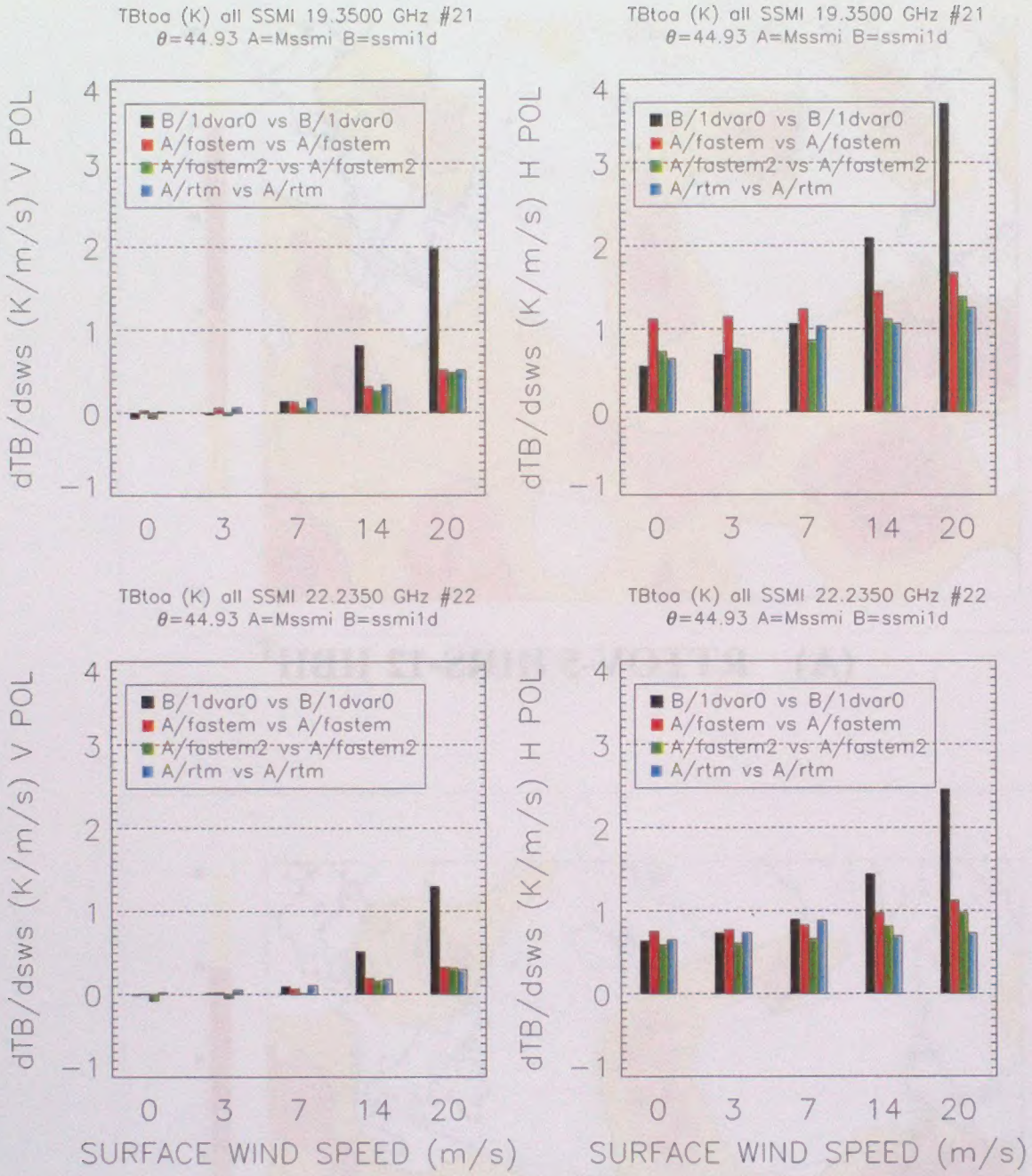

Figure 17: Sensitivity of the brightness temperature at the top of the atmosphere to surface wind speed ($\frac{dTB}{dSWS}$) for the SSM/I 19.35 and 22.235 GHz channel as a function of surface wind speed and for the 4 following models (there are 4 bars for each wind speed): (1) RTSSMI (1dvar0), (2) FASTEM, (3) FASTEM-2 and (4) RTM. The sensitivity was averaged over all profiles of the GARAND26 data set.

End of Report